hpi. Together, these results indicate that the targeting of progeny vRNP to RE is necessary for trafficking of vRNP segments and subsequent efficient infectious virus production.

## vRNPs are coimmunoprecipitated with active/GTP-bound Rab11

The interaction of vRNP with active/GTP-bound Rab11 was examined by immunoprecipitation (Figure 5A). MDCK-Neo, MDCK-F11A-WT, -DN, and -CA cells were infected with influenza virus and post-nuclear supernatants (PNS) were incubated with anti-FLAG mAb, and immunoprecipitated (Figure 5A, lanes 5–8). Western blotting analyses revealed that all protein components of vRNP (PB2, PB1, PA, and NP) were coimmunoprecipitated with the WT and CA mutant FLAG-Rab11A proteins (Figure 5A, lanes 6 and 8, respectively) but not with the DN mutant (Figure 5A, lane 7). Reversely, FLAG-Rab11 CA mutant was coprecipitated, when viral RNP complexes were immunoprecipitated by mAb61A5 (Figure 5B, lane 8). Other viral proteins, such as HA and M1, were not coimmunoprecipitated with FLAG-Rab11A proteins (Figure 5A). These results were in good agreement with our immunofluorescence observations that cytoplasmic HA signals did not colocalize with progeny vRNP signals, when detected by *in situ* hybridization [45] or by mAb61A5 (Figure S2). These results indicate that the transport vesicles for progeny vRNP segments are distinct from those for viral membrane/matrix proteins.

Next, we focused on classes of viral RNAs in the immunoprecipitate, namely vRNA segments with negative polarity and cRNA segments or mRNA with positive polarity (c/mRNA), and classes of RNA segments. We carried out polarity-specific reverse

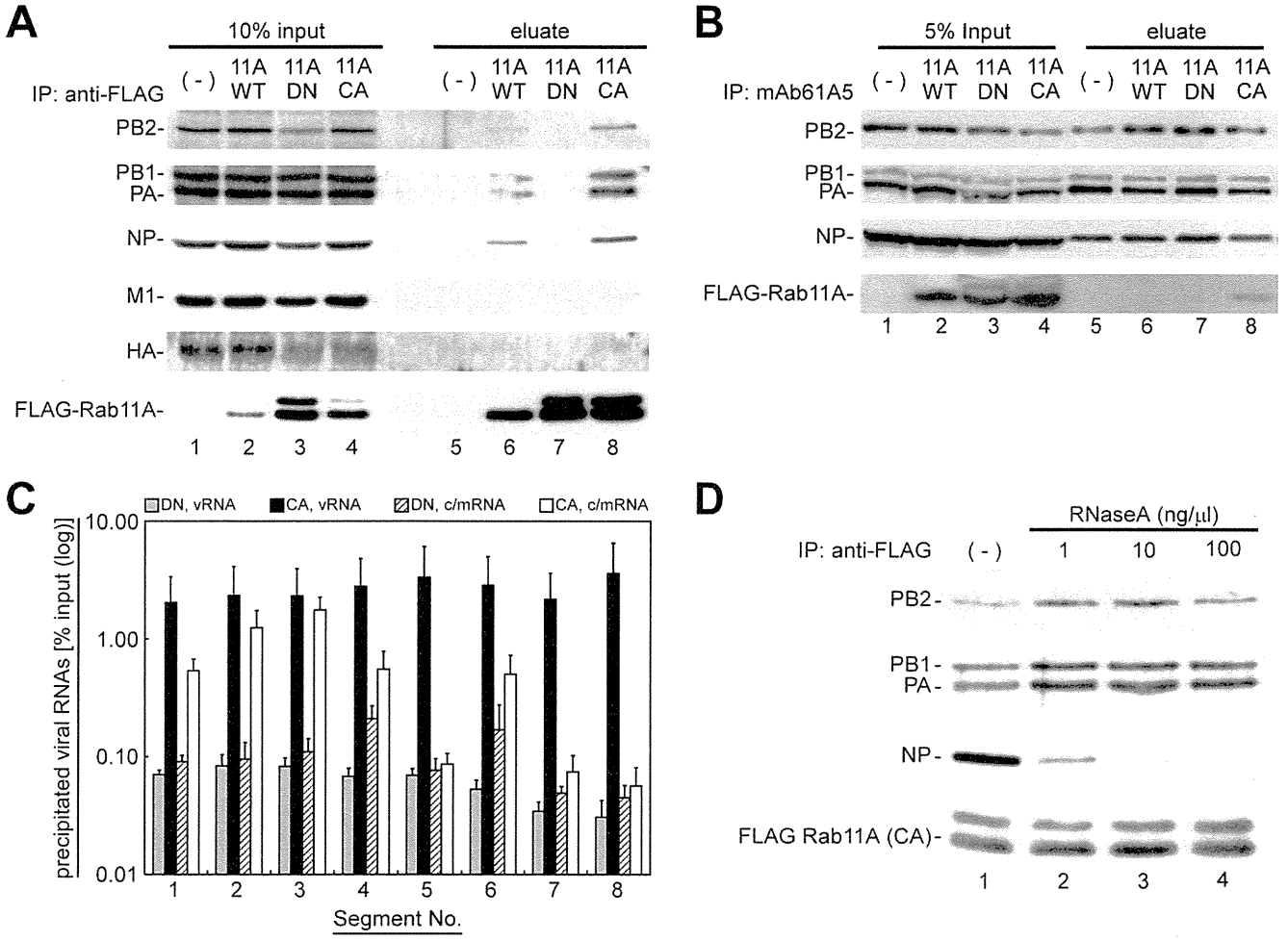


**Figure 5. Coimmunoprecipitation of progeny vRNP segments with active/GTP-bound Rab11A.** (**A**) Coimmunoprecipitation of viral proteins with FLAG-Rab11A and its mutants. MDCK-Neo (lanes 1 and 5), MDCK-F11A-WT (lanes 2 and 6), -DN (lanes 3 and 7), and -CA (lanes 4 and 8) cells were infected with PR8 strain and harvested at 7 hpi. PNS were subjected to immunoprecipitation assays using anti-FLAG mAb, and 10% input (lanes 1–4) and precipitates (lanes 5–6) were analyzed by Western blotting with mouse anti-HA antiserum and anti-FLAG mAb, rabbit anti-PB2, PB1, PA, NP, and M1 antisera. (**B**) Coimmunoprecipitation of FLAG-Rab11 CA mutant with viral RNP complexes. Immunoprecipitation assay was carried out using anti-NP mAb61A5. Precipitates were treated with RNase A and eluates were subjected to Western blotting analysis. (**C**) Coimmunoprecipitation efficiencies of viral RNAs. The amounts of viral RNAs in the immunoprecipitates with anti-FLAG mAb were quantified by polarity-specific reverse transcription followed by segment-specific semiquantitative real-time PCR. Coimmunoprecipitation efficiencies were calculated as percentage of RNA amounts in precipitates relative to those in the input (Figure S3). Segment numbers were indicated at the bottom. Columns indicated the coimmunoprecipitation efficiencies of vRNAs (gray and black columns) and c/mRNAs (hatched and white columns) from MDCK-F11A-DN and -CA. (**D**) Coimmunoprecipitation of vRNP components in the presence of RNase A. Immunoprecipitation assays using infected MDCK-F11A-CA cells were carried out in the absence (lane 1) or the presence of 1, 10, and 100 ng/μl RNase A (lanes 2–4, respectively). Coprecipitated vRNP components (PB2, PB1, PA, and NP) and direct precipitates (FLAG-Rab11A CA) were detected by Western blotting.
doi:10.1371/journal.pone.0021123.g005

transcription followed by segment-specific semiquantitative real-time PCR (Figure 5C). All vRNA segments were coimmunoprecipitated with Rab11A CA mutant at relatively equal efficiency (2.0–3.6% of input vRNA, Figure S3). These precipitates were not observed with the DN mutant (less than 0.1% of input). The data suggest, although do not prove, that vRNA was coimmunoprecipitated as a component of vRNP and that the coimmunoprecipitation depended on a common characteristic of all vRNA segments, such as terminal panhandle structures rather than segment-specific base sequences or segment lengths. Some of c/mRNAs were also coimmunoprecipitated in an active/GTP-bound Rab11-dependent manner. The coimmunoprecipitation efficiencies of c/mRNAs likely depended on their base lengths to some extent.

### Viral heterotrimeric RNA polymerase is the primary component required for Rab11-vRNP interaction

To ascertain the primary component of vRNP required for the interaction with active/GTP-bound Rab11, we carried out immunoprecipitation assays in the absence or the presence of ribonuclease A (RNase A) using the PNS of infected MDCK-F11A-CA cells (Figure 5D). If viral RNA polymerase (PB2, PB1, and PA) bound to the panhandle region of vRNA was the primary component, it should be coimmunoprecipitated with Rab11A even after RNase A treatment, but NP would be dissociated from the complex. Conversely, if NP was the primary target, NP but not viral RNA polymerase would be precipitated. If vRNA of vRNP itself was the primary component, both polymerase and NP would be sensitive to RNase A treatment. Our data show that coimmunoprecipitations of PB2, PB1, and PA with the CA mutant of FLAG-Rab11A were resistance to RNase A treatment and that of NP was apparently sensitive (Figure 5D, compare lane 1 and the others), suggesting that Rab11 interacts with vRNP through viral RNA polymerase, although viral/host factor(s)-mediated interaction cannot be ruled out.

### Overexpression of the Rab binding domains of Rab11 family interacting proteins inhibits localization of vRNP to RE

The Rab family protein is involved in a variety of cellular processes through interaction with specific effector proteins. In the case of Rab11, Rab11 family interacting proteins (Rab11-FIP1 to 5) have been identified as effector proteins (Figure 6A) [57,58,59,60]. The Rab binding domains (RBDs), located at the carboxyl termini of Rab11-FIPs, are relatively conserved among Rab11-FIPs and interact with the switch regions of active form of Rab11 [61,62,63]. The other regions are involved in the effector functions of individual Rab11-FIPs [64,65]. We examined if Rab11-FIP played an important role in the targeting of progeny vRNP to RE. We constructed RBD deletion (ΔRBD) mutants and RBD fragments of Rab11-FIPs and added a FLAG tag to the carboxyl termini of the ΔRBD mutants and monomeric red fluorescent protein, mStrawberry, to the amino termini of the RBD fragments (Figure 6A, FIPnΔRBD-FLAG and mSB-FIPnRBD, n = 1 to 5). Since Rab11-FIP ΔRBD mutants cannot bind with Rab11, overexpression of ΔRBD mutants might inhibit the effector functions of the corresponding endogenous Rab11-FIPs. However, none of Rab11-FIP ΔRBD mutants altered the localization of vRNP to RE (Figure 6B, FIPnΔRBD-FLAG). In contrast, all Rab11-FIP RBD fragments we tested impaired the localization of vRNP to RE (Figure 6B, mSB-FIPnRBD), implying that excess level of RBD expression might disrupt the Rab11-vRNP interaction.

### Apical transport of progeny vRNP depends on the endosomal recycling pathways

It is well known that influenza virus buds at the APM in polarized epithelial cells [23]. Our previous study indicated that vRNP signals were accumulated at the APM in polarized MDCK cells after 6 hpi [45]. Thus, we carefully observed the xz section images of infected MDCK cells. Consistent with the xy images (Figure 6B), marked accumulation of vRNP signals at the APM was not observed when Rab11-FIP RBD fragments were overexpressed (Figure 6C, mSB-FIPnRBD), suggesting that the APM accumulation of cytoplasmic vRNPs is not due to diffusion even though the apical side of nuclear membrane is close to the APM. When observed with Rab11-FIP ΔRBD mutants, we confirmed that class I Rab11-FIP ΔRBD mutants did not impair the APM accumulation of vRNPs (Figure 6C, Rab11-FIP1B/2/5ΔRBD). Interestingly, overexpression of class II Rab11-FIP ΔRBD mutants did not exhibit the APM accumulation of vRNPs (Figure 6C, Rab11-FIP3/4ΔRBD), although these mutants did not inhibit the targeting of vRNPs to RE (Figure 6B). It is plausible that overexpression of nonfunctional Rab11-FIP3/4 mutants disturbed the apical trafficking by disrupting the structural integrity of pericentriolar ERC/RE, as reported previously [66,67]. Altogether, our data suggest that not only targeting of vRNP to RE but also functional apical recycling machinery are both required for membrane trafficking of progeny vRNPs and subsequent particle release.

## Discussion

In this study, we showed that (i) progeny vRNP of influenza A virus was localized at RE and transported along microtubules; (ii) The localization required the interaction between active/GTP-bound Rab11 and a heterotrimeric form of viral RNA-dependent RNA polymerase; and (iii) The Rab11-dependent interaction was required for the targeting of progeny vRNPs to the APM, where virion packaging and budding take place. Very recently, Amorim MJ *et al.* independently reported that cytoplasmic transport of influenza virus RNA genome required Rab11- and microtubule-dependent mechanisms [68]. Their conclusion is in good agreement with our result that genetically unmodified vRNPs moved along the microtubules in living cells. These independent studies confirm the usage of RE for influenza virus vRNP trafficking.

### Live cell imaging using fluorescent-labeled antibody transfection technique, and microtubule-dependent viral transport

For live cell imaging of vRNPs, we have transfected fluorescent-labeled mAb61A5 which preferentially recognized RNP complexes of influenza virus and have demonstrated that vRNP signals move along AcGFP-labeled microtubules rapidly but intermittently in both plus and minus directions (Figures 1 and 2, Videos S1 and S3). Thus, live cell imaging using fluorescent-labeled antibody may have advantages over a conventional technique of tagging with fluorescent protein (i) when the tagging impairs protein functions or trafficking and (ii) when the antibody specifically detects a certain population of protein of interest. This technique does not require special skills and equipments when compared with microinjection. The disadvantages of fluorescent-antibody transfection include the appearance of pseudo-positive signals, as shown in Figures 1 and 2. They are probably antibodies that were endocytosed non-specifically, or aggregated on the plasma membrane or with liposomes. Thus, cotransfection of non-specific control antibody and/or mock infection of inactivated virus are

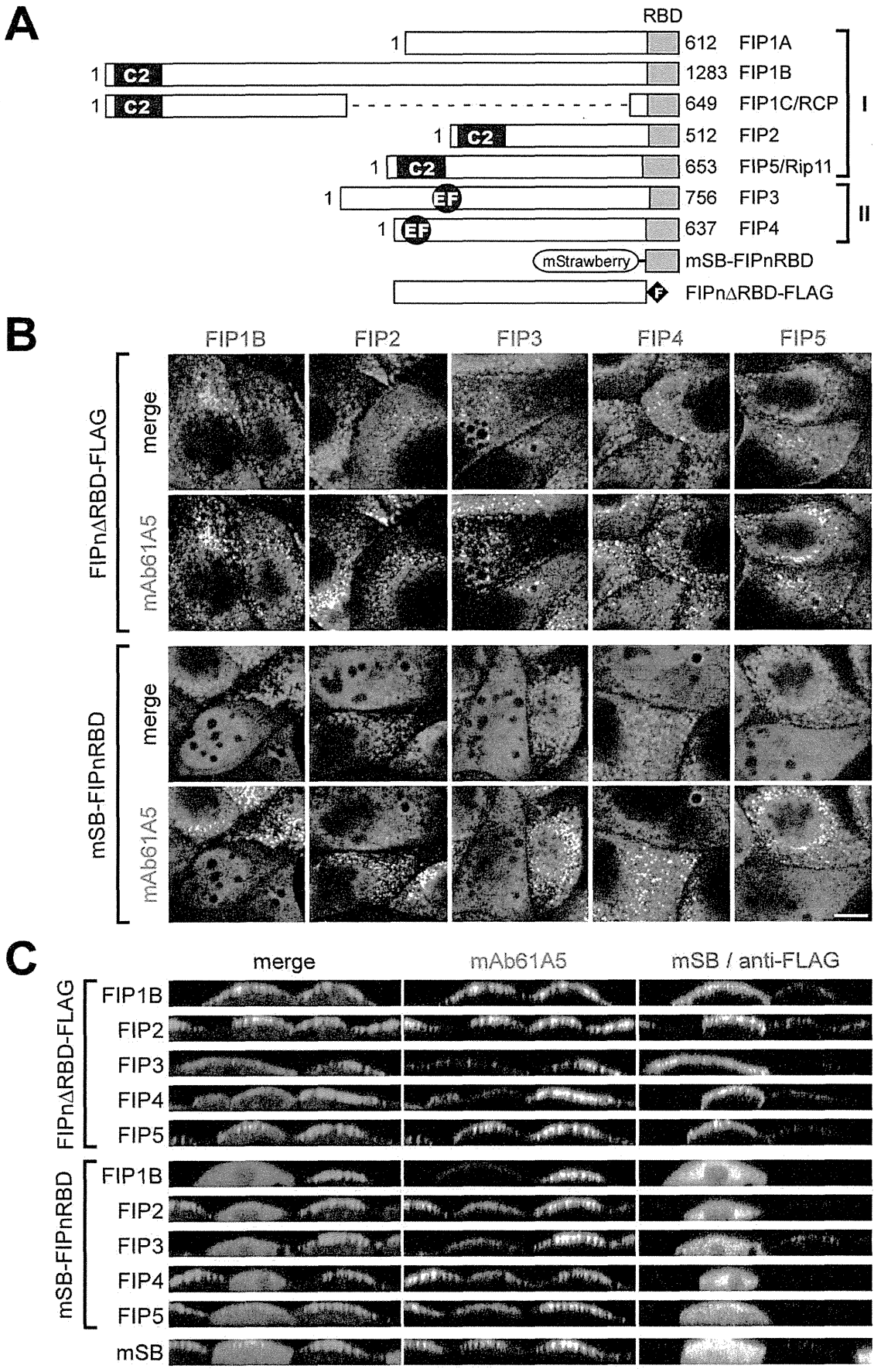
A
RBD
1
612
FIP1A
1
C2
1283
FIP1B
1
C2
649
FIP1C/RCP
I
1
C2
512
FIP2
1
C2
653
FIP5/Rip11
1
EF
756
FIP3
II
1
EF
637
FIP4
mStrawberry
mSB-FIPnRBD
F
FIPnΔRBD-FLAG
B
FIP1B
FIP2
FIP3
FIP4
FIP5
FIPnΔRBD-FLAG
merge
mAb61A5
mSB-FIPnRBD
merge
mAb61A5
C
merge
mAb61A5
mSB / anti-FLAG
FIPnΔRBD-FLAG
FIP1B
FIP2
FIP3
FIP4
FIP5
mSB-FIPnRBD
FIP1B
FIP2
FIP3
FIP4
FIP5
mSB

**Figure 6. Effects of Rab11-FIP deletion mutants on the localization and trafficking of progeny vRNP segments.** (**A**) Schematic representation of the functional domains of human Rab11-FIPs (FIPn). Numerals at both ends indicate amino acid residues. The Rab binding domains (RBD) of individual Rab11-FIPs were indicated as gray boxes. Typical Rab11-FIP1 gene products (FIP1A, -B, and -C/RCP) [96] were shown. The RBD fragment tagged with mStrawberry at the amino terminus (mSB-FIPnRBD) and the RBD deletion mutant containing a FLAG epitope tag at the carboxyl terminus (FIPnΔRBD-FLAG) were also illustrated. C2, C2-domain; EF, EF-hand domain. (**B**) Localization of progeny vRNPs in infected MDCK cells transiently expressing Rab11-FIP deletion mutants. Rab11-FIPs with deletion of RBD (upper two rows) and RBD fragments (lower two rows) were visualized using anti-FLAG mAb and mSB (red), respectively. Progeny vRNPs were also visualized using anti-NP mAb61A5 (green). Confocal merged images (odd rows) and vRNP-channel images (even rows) are shown. All images are shown at the same magnification. Scale bar = 10 μm. (**C**) Polarized localization of progeny vRNP. XZ sections of polarized MDCK cells. Nuclei were stained with DAPI (blue) and shown in merged images (left images).
doi:10.1371/journal.pone.0021123.g006

required to distinguish true signals from pseudo-positives. Another disadvantage would be a possible reduction in velocity because of large complex formation of antigen and antibody.

Previous studies indicated that HSV moved in axon of cultured nerve cell at 2–3 mm/h [69] and that organelles containing HSV capsids moved on *in vitro*-reconstituted microtubules at a mean velocity of 0.58 μm/s [70]. Sendai virus vRNP was visualized by tagging with fluorescent protein to L protein and velocity of the RE-dependent vRNP movement was calculated at subsecond temporal resolution (0.41–1.04 μm/s) [71]. These velocities were ostensibly comparable to the mean velocity of influenza virus progeny vRNPs observed in our study (Figure 1B, approximately 1.45 μm/s). Since cargos which are transported along microtubules by membrane vesicles moves rapidly but intermittently in both directions, subsecond temporal resolution must be required for accurate instantaneous velocity of their transport. A very recent report demonstrated that a fraction of reconstituted influenza virus vRNP showed saltatory movement at an average of 0.81 μm/s [68]. This mean velocity is slightly slower than but still comparable with our mean velocity of genetically unmodified vRNP in infected cells. Relatively lower temporal resolution (approximately every 4s), tagging with GFP, and/or the elapsed time from the transfection (24 hours posttransfection) may cause the velocity reduction observed in their study.

## Localization of progeny vRNP to RE via interaction between viral RNA polymerase and Rab11

Previous studies on transient coexpression of three subunits of viral RNA polymerase (PB2, PB1, and PA) have indicated that hetero-trimerization of the subunits takes place in the nucleus but not in the cytoplasm, showing a limited localization of heterotrimeric viral RNA polymerase in the nucleus [72,73,74]. In the infected cell, the heterotrimeric viral RNA polymerase is incorporated into progeny vRNP and then exported to the cytoplasm by CRM1-dependent nuclear export system [75], whereas cRNP which serves a template for vRNA synthesis remains in the nucleus [12]. These studies suggest that most of the heterotrimeric viral RNA polymerase in the cytoplasm exists as a constituent of progeny vRNP. In this study, our immunoprecipitation analysis with RNase A treatment revealed that active/GTP-bound Rab11 interacted with vRNP through the viral RNA polymerase but not NP or vRNA (Figure 5D), although it remains to be elucidated whether the interaction is direct or not. If a certain subunit or heterodimer could solely interact with Rab11, it would also be transported to the APM. However, it has been well known that not only singly expressed subunits but also coexpressed three subunits did not accumulate at the plasma membrane [73,74]. Thus, we reasoned that the heterotrimeric viral RNA polymerase in vRNP might serve as a marker for RE-dependent apical transport of progeny vRNP, since Rab11, a resident of RE, binds to viral RNA polymerase. It has been suggested that enzymatic/structural state of viral RNA polymerase is probably altered by classes of associated RNAs, e.g., single-stranded RNA, panhandle region of vRNA, or that of cRNA [12,76,77]. The state of viral RNA polymerase may similarly serve as a marker for targeting of vRNP to RE and excluding of viral mRNP containing single-stranded viral mRNA, if present in the cytoplasm. We are currently investigating whether active/GTP-bound Rab11 directly interacts with a certain class of viral RNA polymerase, or another viral/host factor(s) is involved. Amorim MJ *et al.* have suggested that the Rab11-vRNP interaction is due to Rab11-PB2 subunit interaction [68]. In their study, coexpression of GFP-tagged CA Rab11 with PB2, PB1, PA, or NP and subsequent affinity precipitation of GFP-Rab11 resulted in the coprecipitation of PB2 but not the other viral components. Although it remains to be elucidated why PB2 subunit could solely interact with active/GTP-bound Rab11 in the cytoplasm, it is possible that PB2 in the heterotrimeric viral RNA polymerase complex in a certain enzymatic/structural state participates in the Rab11-vRNP interaction.

## A model for a higher-order assembly of progeny vRNP segments on a Rab11-positive membrane

Recent studies have suggested that viral membrane/matrix proteins of some viruses traffic via endosomal pathways [13,14]. However, the intracellular trafficking of viral inner components has long been less understood. In this study, we identified RE as a target compartment of influenza virus progeny vRNP. A possible explanation for the utilization of RE is that the surface of RE is a place for a higher-order assembly of vRNP segments (for review, see [78]). From studies with defective-interfering viral RNAs [79,80,81], it has been widely accepted that eight distinct segments of progeny vRNP are selectively packaged into a virion. Recent reports have shown that the approximately 150 to 200 base sequences at both termini of vRNA segments are responsible for their selective packaging into virions [82,83], although it has not been demonstrated whether the putative inter-vRNP base pairing through the terminal regions is the molecular basis of the selective assembly and/or packaging. If it was the case, intracellular localization, local concentration, and spatial orientation of the terminal regions would be of great importance.

We propose the models for a higher-order assembly of vRNP segments (Figure 7). The most likely scenario (Figure 7B) would be that (i) the progeny vRNP segments bind to RE membrane (Figure 3, panels A and E) through interaction of active/GTP-bound Rab11 and heterotrimeric viral RNA polymerase (Figure 5D), followed by trafficking to the APM along microtubules (Figure 2). (ii) Because viral RNA polymerase is associated with the panhandle region of vRNA where is close to the sequences necessary for genome packaging (gray box), these terminal regions are concentrated and aligned in the same orientation on the RE membrane and later at the APM. (iii) By lateral diffusion, each vRNP segment slides on the membrane surface relatively freely to seek the others. This mild spatial restriction may allow a higher-order assembly of vRNP segments in a "try and select" manner, leading to packaging of eight vRNP

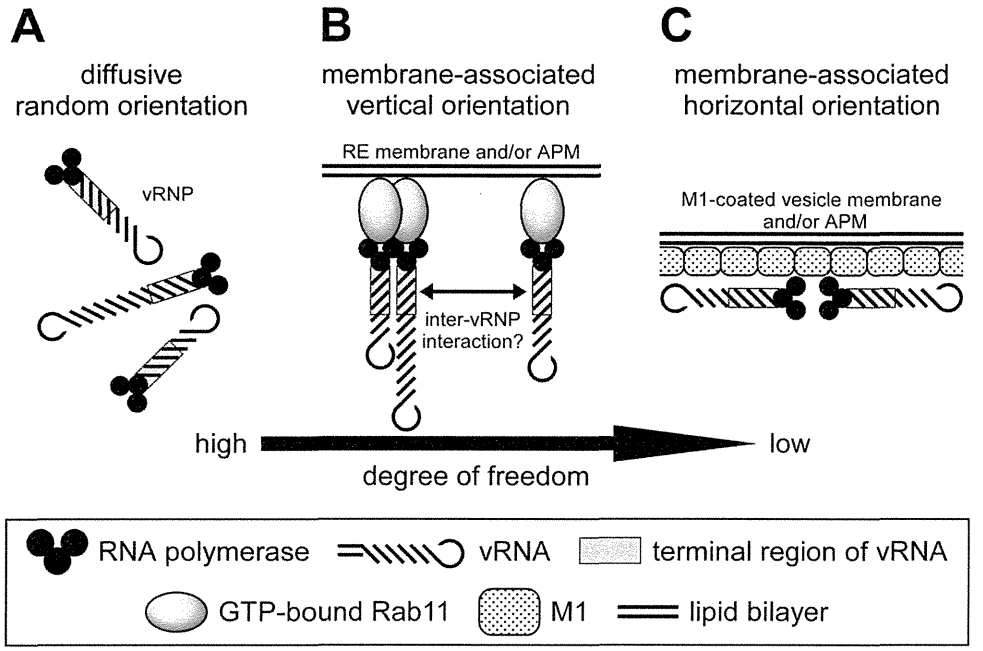


**Figure 7. Models for spatial orientation of vRNP segments toward a higher-order assembly.** Putative spatial orientations of progeny vRNP segments in the cytoplasm were illustrated. (**A**) Diffusive random orientation model, (**B**) membrane-associated vertical orientation model may occur on RE and/or beneath the APM, and (**C**) membrane-associated horizontal orientation model may occur on a vesicle and/or beneath the APM precoated with M1. Details were described in the Discussion section.
doi:10.1371/journal.pone.0021123.g007

segments into a virion, as observed by electron microscopy [84,85].

If vRNP segments were freely diffusible in the cytosol (Figure 7A), the frequency of putative inter-vRNP interaction in a correct orientation would be very low. In fact, coexpressed with the DN mutant of Rab11 and Rab11-FIP RBD fragments (Figure 4A and 6B, respectively), vRNPs remained diffuse and were not seen as puncta, suggestive of a failure of a higher-order assembly of vRNP segments. Consistently, the production of infectious virions from the cells expressing the DN mutant was markedly decreased (Figure 4B), although perturbation of Rab11-dependent budding events cannot be ruled out [38]. An alternative model would be assembly of vRNP segments on M1-precoated vesicle/membrane (Figure 7C) as suggested previously (for review, see [86]). If NP and/or vRNA in a vRNP interacted directly with M1 [87,88,89], vRNP segments would be immobilized on the M1-coated membrane and fail to assemble each other. Recent electron microscopic analysis has suggested no such a tight association of vRNP with the electron-dense M1 layer in virions [84,85]. Neither progeny vRNP signals detected by mAb61A5 nor by FISH analysis colocalized with HA/M1 antigens in the cytoplasm (Figure S2 and [45]). These results suggest that progeny vRNP and HA/M1 are transported independently through distinct apical transport pathways [90].

## Rab11, a key player in trafficking of non-membrane-bound cytoplasmic viral/cellular factors

In the past three decades, endosomal recycling has been extensively investigated. The majority of cargos analyzed are membrane-bound proteins/complexes and membrane lipids, e.g., transferrin-transferrin receptor complexes and endocytic transport to the cleavage furrow during cytokinesis. The well-known non-membrane-bound cytoplasmic cargos of RE are Rab11 effectors and motor proteins. Recent virological studies suggest independently the utilization of RE for viral trafficking and egress: cytoplasmic transport of hantavirus [91], apical budding of RSV [35,92], cytoplasmic envelopment of human cytomegalovirus [93], and budding of influenza A virus [38]. It has been reported that the RE machinery is also used for vRNP trafficking of Sendai virus [71] and most recently for the trafficking of the influenza virus RNA genome [68], independently of our study. In this study, we reported that Rab11 recognized a non-membrane-bound molecule, i.e., progeny vRNP, and transported from the perinuclear region to the APM via RE. Collectively, these data strongly suggest that the utilization of Rab11-driven endosomal recycling system is a common transport mechanism of viral and possibly cellular non-membrane-bound cytoplasmic cargos. Budding of influenza A virus has been shown to occur independently of the ESCRT machinery [36,37] but to require the Rab11-mediated machinery [38], suggesting that influenza virus may require a Rab11-related molecule(s) for virion release. It is tempting to speculate that vRNP segments and a factor(s) necessary for virion budding/pinching-off meet on a Rab11-positive RE and are transported together to the APM. Viral M2 protein is a candidate of such a factor since it has been reported that M2 protein mediates ESCRT-independent membrane scission and knock-down of Rab11 leads to a statistically significant reduction in the levels of M2 from the cell surface [94].

Our present study provides an outline of intracellular trafficking of influenza viral replication complex, vRNP, from the nucleus, a site of viral genome replication, to the APM, a site of genome packaging and virion budding. However, many elementary steps of the trafficking remain to be elucidated. For examples, an intracellular site where progeny vRNPs initially ride on Rab11-positive RE and motor proteins involved in the apical trafficking of vRNPs need to be identified. Investigation of these elementary steps will reveal precise molecular mechanisms of apical trafficking and a higher-order assembly of progeny vRNP segments for genome packaging. Our

study may also provide a clue to the transport mechanisms of host cellular non-membrane-bound cytoplasmic cargos such as mRNP trafficking followed by local protein translation.

## Materials and Methods

Materials and Methods for antibodies, DNA construction, establishment of cell lines, and immunofluorescent microscopy were described in Materials and Methods S1. Oligonucleotide sequences used for DNA construction were described in Tables S2, S3, S4 and S5.

### Live cell imaging

MDCK cells were cultured in Dulbecco's modified Eagle medium (DMEM, Cat. No. D5796, Sigma-Aldrich, USA) containing 10% fetal bovine serum (FBS) on ϕ35 mm glass-bottom dishes and infected with influenza virus A/Puerto Rico/8/34 (PR8) strain at moi of 3 for 1 h. Residual viral inoculum was digested with 80 μg/ml of acetyl-trypsin in serum-free medium (Opti-MEM I, Life Technologies, USA) for 2 h and followed by masking with 0.2 mg/ml of unlabeled mAb61A5 for 30 min. At 3.5 hpi, 400 ng of Alexa Fluor 568 (AF568)-labeled mAb61A5 was transfected together with 400 ng of AF488-labeled non-specific mouse immunoglobulin (control antibody), using protein transfection reagent (Ab-DeliverIN, OZ Biosciences, France) according to the manufacturer's instruction. At 7 hpi, the medium was exchanged to DMEM for live cell imaging (Cat. No. 21063-029, Life Technologies) containing 10% FBS.

Live cell imaging was performed using a fluorescence microscope (IX71, Olympus Optical, Japan) equipped with an oil immersion objective lens (Plan Apo N, 60x, 1.42NA, Olympus), a stage top incubation chamber (Tokai HIT, Japan), a microlens-enhanced Nipkow-disk confocal scanner unit (CSU-X1, Yokogawa Electric, Japan), an optical filter wheel controller, and an electron multiplying CCD camera (Luca, Andor Technology, UK). For pseudo-positive signals, both fluorescent images with mAb61A5 and control antibody were acquired alternately (0.25 to 0.50 s exposure/image) with Ar laser excitation (488 or 568 nm) and were merged (Figure 1A, merge; Video S1, the first color part). Immediately after the dual-color acquisition, single channel acquisition of mAb61A5 images was carried out at 0.25 s exposure/image (Video S1, the second gray scale part). Sequential images were processed by using ImageJ software [95] as follows: (i) bleach correction, (ii) subtraction of a time projection image of mean intensity from fluorescence images at each time point, (iii) contrast correction (Video S1, the third part), and (iv) tracking of punctate fluorescent signals by using MTrackJ plugin created by Eric Meijering (http://www.imagescience.org/meijering/software/mtrackj/) (Video S1, the fourth part with trajectories).

### Kinetic analysis of fluorescent signals

Coordinates of vRNP signals at each time point were obtained from trajectories. An instantaneous velocity ($v_n$, n means a frame number) and a vector ($\boldsymbol{V}_n$) of a signal at each time point were calculated from coordinates n ($x_n$, $y_n$), n+1 ($x_{n+1}$, $y_{n+1}$), and a frame interval (0.25 s). One motile event was defined as a single unidirectional movement of a signal, when the movement from a start point (frame number s) to an end point (frame number e) fulfills the following conditions: (i) $v_n > 0.13$ μm/s (n is s to e-1), (ii) a relative angle between vectors $\boldsymbol{V}_n$ and $\boldsymbol{V}_{n+1}$ $< \pm 60°$ (n is s to e-2), and (iii) at least four sequential time points, i.e., a duration is no fewer than 0.75 s when frame interval is 0.25 s. The threshold velocity (0.13 μm/s) was determined by the mean of instantaneous velocities of vRNP signals in pausing conditions. The angle threshold (±60°) was estimated from the maximum curvature of microtubules observed by immunofluorescence microscopy and the maximum velocity 10 μm/s we tentatively assigned. Mean and maximum of instantaneous velocities ($V_{mean}$ and $V_{max}$, respectively) and migration length of one motile event were calculated (Table S7) and plotted as histograms.

### Immunoprecipitation

MDCK-Neo, MDCK-F11A-WT, -DN, and -CA cells were seeded into ϕ10 cm dishes ($3\times10^6$ cells/dish). After incubation for 12 h, cells were infected with influenza virus PR8 strain at moi of 1 for 1 h. At 7 hpi, cells were harvested with 1 ml of cold PBS containing 0.1% Tween-20 (PBS-T), 1 mM DTT, 0.1 mM GTPγS (JENA Bioscience, Germany), 100 ng/μl of BSA, 0.5 U/μl of RNase inhibitor (Toyobo, Japan), and protease inhibitor cocktail (Cat. No. 25955-11, Nacalai Tesque, Japan). Cells were passed through 26G needle 20 strokes and the PNS was isolated by centrifugation at 4°C, at 1,000× g for 10 min. One milliliter of PNS was mixed with 20 μg of anti-FLAG mAb and incubated on ice for 1 h. The PNS was subsequently mixed with pre-blocked 20 μl packed-volume (p.v.) of Protein G Mag Sepharose (GE Healthcare, UK) and rotated at 4°C for 2 h. After being washed twice with PBS-T, immunoprecipitates were eluted twice with 50 μl of PBS-T containing 150 ng/μl of 3×FLAG peptide (Sigma-Aldrich) for 30 min (total 60 min and 100 μl of eluate). The eluate and PNS were analyzed by Western blotting. Similarly, immunoprecipitation of viral RNP complexes were carried out with 20 μg of anti-NP mAb61A5 and eluted twice with 25 μl of PBS-T containing 100 ng/μl RNase A at 25°C for 30 min (total 60 min and 50 μl of eluate).

For RNase sensitivity assay, PNS of infected MDCK-F11A-CA cells were similarly prepared except for RNase inhibitor. Following addition of anti-FLAG mAb to the PNS, 250 μl of aliquots were incubated with 0 to 100 ng/μl of RNase A at 25°C for 1 h and precipitated by using 5 μl p.v./assay of Protein G Mag Sepharose at 25°C for 2 h. Elution was carried out twice with 25 μl of elution buffer at 25°C for 30 min (total 60 min and 50 μl of eluate).

### Reverse transcription and semiquantitative real-time PCR

RNA was isolated from immunoprecipitation eluate (Fig. 5C) and PNS (Figure S3) by using RNeasy mini kit (Qiagen, Germany). Equal volume of each RNA sample was used for reverse transcription (ReverTra Ace qPCR RT Kit, Toyobo) in the presence of a primer mixture containing 2 pmol each of eight segment-specific primers, which is either for negative- (vRNA) or positive-sense (c/mRNA) influenza virus RNAs (Table S6). Semiquantitative real-time PCR (qPCR) was carried out (SYBR Premix Ex Taq II and Real Time PCR System TP800, Takara Bio, Japan) in the presence of each segment-specific qPCR primer pair (reverse transcription product ×8 qPCR reactions). Threshold cycles (Ct) were obtained by second derivative maximum method.

For the standard DNA of segment-specific qPCR, short cDNA fragments to individual viral RNA segments were amplified using qPCR primer pairs, concatenated, and cloned into pBluescript-SK(+) (Agilent Technologies, USA) (see Materials and Methods S1 and Figure S1B). The resultant plasmid (pBSPR8qPCRSTD) has one copy each of eight qPCR target sequences. Standard curves for Ct values of individual targets vs. cDNA concentrations were obtained using ten-fold dilutions of this standard DNA (0.0001 to 0.1 fmol/reaction) and were used for relative quantification of reverse-transcribed cDNA segments.

## Supporting Information

**Figure S1 DNA construction of expression vectors and the standard DNA plasmid for qPCR.** (A) DNA sequences of pCANeoHA and pCANeoAcGFP-MCS. The DNA sequences corresponding to the region between two *Eco*R I sites of original pCAGGS were shown. The positions of cloning sites, HA epitope tag, and AcGFP tag were indicated. Amino acid sequences were also shown. (B) Construction scheme of the qPCR standard plasmid (pBSPR8qPCRSTD) containing one copy each of eight distinct target sequences. Numerals, segment numbers of the influenza virus genome; white circles, 5′-phosphorylated. Details were described in Materials and Methods S1.
(TIF)

**Figure S2 Localizations of progeny vRNP and hemagglutinin in the cytoplasm.** MDCK cells were infected with PR8 strain for 1 h and 20 μM of brefeldin A (BFA), a vesicular transport inhibitor, was added at 4 h postinfection (hpi). Following fixation at 7 hpi, immunofluorescence staining was carried out as follows: (i) staining with anti-HA mAb and Alexa Fluor 488 dye (AF488)-conjugated anti-mouse Ig, (ii) post-fixation with 4% paraformaldehyde and blocking with non-specific mouse Ig, and (iii) staining with AF568-conjugated mAb61A5. Cells were observed with a confocal laser scanning microscope. Areas in white boxes were enlarged. In the presence of brefeldin A, membrane transport of HA was partially inhibited and a fraction of HA accumulated at the perinuclear region. An arrowhead shows a filamentous vRNP signal observed in the presence of BFA. Bars are 20 μm and 5 μm, respectively.
(TIF)

**Figure S3 Molar ratios of viral negative/positive-sense RNA segments in PNSs of infected MDCK-F11A-DN/CA cells.** Total RNAs were purified from infected cells and polarity-specific reverse transcription followed by segment-specific semi-quantitative real-time PCR was carried out. Amounts of the cDNAs reverse-transcribed from viral RNAs were quantified using standard plasmid DNA containing single copy of each target sequence (pBSPR8qPCRSTD). Segment numbers were indicated at the bottom. Columns indicated the molar ratio of vRNAs (gray and black columns) and c/mRNAs (hatched and white columns) from MDCK-F11A-DN and -CA, when the segment 1 vRNA from MDCK-F11A-DN was set at 1.0.
(TIF)

**Table S1 List of Analyzed Rab Family Proteins and Their Cloning Information.**
(DOC)

**Table S2 Oligonucleotide Sequences. Used for the Cloning of Rab Family Proteins.**
(DOC)

**Table S3 Oligonucleotide Sequences Used for the Construction of Dominant Negative and Constitutively Active Mutants of Human Rab11A.**
(DOC)

**Table S4 Oligonucleotide Sequences Used for AcGFP- or FLAG-tagged Rab Family Protein Expression Vectors.**
(DOC)

**Table S5 Oligonucleotide Sequences Used for the Construction of Rab11-FIPs Deletion Mutant Expression Vectors.**
(DOC)

**Table S6 Oligonucleotide Sequences Used for Polarity-specific Reverse Transcription and Segment-specific Semiquantitative PCR.**
(DOC)

**Table S7 Mean and Maximum Velocities and Migration Lengths of Individual Motile Events.**
(DOC)

**Video S1 A representative live cell imaging and tracking of cytoplasmic progeny vRNP signals.** Live cell imaging of infected MDCK cells (Figure 1A) was carried out as described in the Materials and Methods section. Acquired images were processed, analyzed, and encoded to a movie containing concatenated four parts. The first color part contains 25 of merged images (red, mAb61A5 channel; green, control antibody channel). Each of single channel images was acquired alternately at 250 ms exposure. The second gray-scale part contains 100 images acquired at 250 ms exposure for 25 seconds at single mAb61A5 channel, immediately after the dual-color acquisition. The third part of the movie is post-processing images of the second part. The image processing procedure was described in the Materials and Methods section. The last part is the signal tracking by using ImageJ software and MTrackJ plugin (created by Eric Meijering, http://www.imagescience.org/meijering/software/mtrackj/). Individual signals were tracked manually (90 tracks). Track numbers, trajectories, and current position of vRNP signals were indicated on the post-processing images with numerals, colored lines, and blank circles, respectively. Elapsed times were also indicated.
(MPG)

**Video S2 Live cell imaging of mock-infected MDCK cells.** MDCK cells were infected with influenza A virus PR8 strain (right half) or mock-infected with heat-inactivated virus (left half). For live cell imaging, each of single channel images (red, mAb61A5 channel; green, control antibody channel) was acquired alternately at 500 ms exposure/image for 24 seconds and then merged. Bleach correction and contrast correction were carried out.
(MPG)

**Video S3 Live cell imaging of infected MDCK cells expressing AcGFP-α-tubulin.** MDCK-Tub cells, constitutively expressing AcGFP-α-tubulin, were infected with influenza A virus PR8 strain (Figure 2). For live cell imaging, each of single channel images (red, mAb61A5 channel; green, control antibody and AcGFP channel) was acquired alternately at 300 ms exposure/image for 60 seconds and then merged. Bleach correction and contrast correction were carried out. Cropped area (shown in Figure 2B) was encoded as a movie containing concatenated merged images, mAb61A5 channel images, and control antibody/AcGFP channel images. Elapsed times were indicated.
(MPG)

**Materials and Methods S1** Details of the antibodies utilized in this study and methods for DNA construction, establishment of cell lines, and immunofluorescent microscopy were described.
(DOC)

## Acknowledgments

We thank to Drs. Paul Digard, Emily A. Bruce, and Maria Joao Amorim (University of Cambridge, Cambridge, United Kingdom) for the meaningful discussion, and Drs. Ken Watanabe (Nagasaki University, Nagasaki, Japan) and Takayuki Nagai (Kitasato University, Tokyo, Japan) for the generous gifts of rabbit anti-M1 (to KW) and mouse anti-HA polyclonal antisera (to TN).

## Author Contributions

Conceived and designed the experiments: FM KN YM. Performed the experiments: FM TS SJ AK. Analyzed the data: FM TS SJ AK. Contributed reagents/materials/analysis tools: TO KN YM. Wrote the paper: FM YM.

## References


1. Thomas JA, Gorelick RJ (2008) Nucleocapsid protein function in early infection processes. Virus Res 134: 39–63.
2. Brown DT, Westphal M, Burlingham BT, Winterhoff U, Doerfler W (1975) Structure and composition of the adenovirus type 2 core. J Virol 16: 366–387.
3. Black BC, Center MS (1979) DNA-binding properties of the major core protein of adenovirus 2. Nucleic Acids Res 6: 2339–2353.
4. Portela A, Digard P (2002) The influenza virus nucleoprotein: a multifunctional RNA-binding protein pivotal to virus replication. J Gen Virol 83: 723–734.
5. Desselberger U, Racaniello VR, Zazra JJ, Palese P (1980) The 3′ and 5′-terminal sequences of influenza A, B and C virus RNA segments are highly conserved and show partial inverted complementarity. Gene 8: 315–328.
6. Hsu MT, Parvin JD, Gupta S, Krystal M, Palese P (1987) Genomic RNAs of influenza viruses are held in a circular conformation in virions and in infected cells by a terminal panhandle. Proc Natl Acad Sci U S A 84: 8140–8144.
7. Compans RW, Content J, Duesberg PH (1972) Structure of the ribonucleoprotein of influenza virus. J Virol 10: 795–800.
8. Murti KG, Webster RG, Jones IM (1988) Localization of RNA polymerases on influenza viral ribonucleoproteins by immunogold labeling. Virology 164: 562–566.
9. Klumpp K, Ruigrok RW, Baudin F (1997) Roles of the influenza virus polymerase and nucleoprotein in forming a functional RNP structure. EMBO J 16: 1248–1257.
10. Coloma R, Valpuesta JM, Arranz R, Carrascosa JL, Ortin J, et al. (2009) The structure of a biologically active influenza virus ribonucleoprotein complex. PLoS Pathog 5: e1000491.
11. Shapiro GI, Gurney T, Jr., Krug RM (1987) Influenza virus gene expression: control mechanisms at early and late times of infection and nuclear-cytoplasmic transport of virus-specific RNAs. J Virol 61: 764–773.
12. Tchatalbachev S, Flick R, Hobom G (2001) The packaging signal of influenza viral RNA molecules. RNA 7: 979–989.
13. Sodeik B (2000) Mechanisms of viral transport in the cytoplasm. Trends Microbiol 8: 465–472.
14. Radtke K, Dohner K, Sodeik B (2006) Viral interactions with the cytoskeleton: a hitchhiker's guide to the cell. Cell Microbiol 8: 387–400.
15. Sodeik B, Ebersold MW, Helenius A (1997) Microtubule-mediated transport of incoming herpes simplex virus 1 capsids to the nucleus. J Cell Biol 136: 1007–1021.
16. Bukrinskaya A, Brichacek B, Mann A, Stevenson M (1998) Establishment of a functional human immunodeficiency virus type 1 (HIV-1) reverse transcription complex involves the cytoskeleton. J Exp Med 188: 2113–2125.
17. Marsh M, Bron R (1997) SFV infection in CHO cells: cell-type specific restrictions to productive virus entry at the cell surface. J Cell Sci 110(Pt 1): 95–103.
18. Wang K, Huang S, Kapoor-Munshi A, Nemerow G (1998) Adenovirus internalization and infection require dynamin. J Virol 72: 3455–3458.
19. Li E, Stupack D, Bokoch GM, Nemerow GR (1998) Adenovirus endocytosis requires actin cytoskeleton reorganization mediated by Rho family GTPases. J Virol 72: 8806–8812.
20. Matlin KS, Reggio H, Helenius A, Simons K (1981) Infectious entry pathway of influenza virus in a canine kidney cell line. J Cell Biol 91: 601–613.
21. Lakadamyali M, Rust MJ, Babcock HP, Zhuang X (2003) Visualizing infection of individual influenza viruses. Proc Natl Acad Sci U S A 100: 9280–9285.
22. O'Neill RE, Jaskunas R, Blobel G, Palese P, Moroianu J (1995) Nuclear import of influenza virus RNA can be mediated by viral nucleoprotein and transport factors required for protein import. J Biol Chem 270: 22701–22704.
23. Rodriguez Boulan E, Sabatini DD (1978) Asymmetric budding of viruses in epithelial monlayers: a model system for study of epithelial polarity. Proc Natl Acad Sci U S A 75: 5071–5075.
24. Roberts SR, Compans RW, Wertz GW (1995) Respiratory syncytial virus matures at the apical surfaces of polarized epithelial cells. J Virol 69: 2667–2673.
25. Fuller S, von Bonsdorff CH, Simons K (1984) Vesicular stomatitis virus infects and matures only through the basolateral surface of the polarized epithelial cell line, MDCK. Cell 38: 65–77.
26. Mettenleiter TC, Klupp BG, Granzow H (2009) Herpesvirus assembly: an update. Virus Res 143: 222–234.
27. Greber UF, Way M (2006) A superhighway to virus infection. Cell 124: 741–754.
28. Schwartz SL, Cao C, Pylypenko O, Rak A, Wandinger-Ness A (2007) Rab GTPases at a glance. J Cell Sci 120: 3905–3910.
29. Stenmark H (2009) Rab GTPases as coordinators of vesicle traffic. Nat Rev Mol Cell Biol 10: 513–525.
30. Garrus JE, von Schwedler UK, Pornillos OW, Morham SG, Zavitz KH, et al. (2001) Tsg101 and the vacuolar protein sorting pathway are essential for HIV-1 budding. Cell 107: 55–65.
31. Chen BJ, Lamb RA (2008) Mechanisms for enveloped virus budding: can some viruses do without an ESCRT? Virology 372: 221–232.
32. Patton GS, Morris SA, Chung W, Bieniasz PD, McClure MO (2005) Identification of domains in gag important for prototypic foamy virus egress. J Virol 79: 6392–6399.
33. Stange A, Mannigel I, Peters K, Heinkelein M, Stanke N, et al. (2005) Characterization of prototype foamy virus gag late assembly domain motifs and their role in particle egress and infectivity. J Virol 79: 5466–5476.
34. Schmitt AP, Leser GP, Morita E, Sundquist WI, Lamb RA (2005) Evidence for a new viral late-domain core sequence, FPIV, necessary for budding of a paramyxovirus. J Virol 79: 2988–2997.
35. Utley TJ, Ducharme NA, Varthakavi V, Shepherd BE, Santangelo PJ, et al. (2008) Respiratory syncytial virus uses a Vps4-independent budding mechanism controlled by Rab11-FIP2. Proc Natl Acad Sci U S A 105: 10209–10214.
36. Chen BJ, Leser GP, Morita E, Lamb RA (2007) Influenza virus hemagglutinin and neuraminidase, but not the matrix protein, are required for assembly and budding of plasmid-derived virus-like particles. J Virol 81: 7111–7123.
37. Bruce EA, Medcalf L, Crump CM, Noton SL, Stuart AD, et al. (2009) Budding of filamentous and non-filamentous influenza A virus occurs via a VPS4 and VPS28-independent pathway. Virology 390: 268–278.
38. Bruce EA, Digard P, Stuart AD (2010) The Rab11 pathway is required for influenza A virus budding and filament formation. J Virol 84: 5848–5859.
39. Hollinshead M, Rodger G, Van Eijl H, Law M, Hollinshead R, et al. (2001) Vaccinia virus utilizes microtubules for movement to the cell surface. J Cell Biol 154: 389–402.
40. Rietdorf J, Ploubidou A, Reckmann I, Holmstrom A, Frischknecht F, et al. (2001) Kinesin-dependent movement on microtubules precedes actin-based motility of vaccinia virus. Nat Cell Biol 3: 992–1000.
41. Ward BM, Moss B (2001) Vaccinia virus intracellular movement is associated with microtubules and independent of actin tails. J Virol 75: 11651–11663.
42. Cui ZQ, Zhang ZP, Zhang XE, Wen JK, Zhou YF, et al. (2005) Visualizing the dynamic behavior of poliovirus plus-strand RNA in living host cells. Nucleic Acids Res 33: 3245–3252.
43. Santangelo PJ, Bao G (2007) Dynamics of filamentous viral RNPs prior to egress. Nucleic Acids Res 35: 3602–3611.
44. Momose F, Kikuchi Y, Komase K, Morikawa Y (2007) Visualization of microtubule-mediated transport of influenza viral progeny ribonucleoprotein. Microbes Infect 9: 1422–1433.
45. Jo S, Kawaguchi A, Takizawa N, Morikawa Y, Momose F, et al. (2010) Involvement of vesicular trafficking system in membrane targeting of the progeny influenza virus genome. Microbes Infect 12: 1079–1084.
46. Lee JR, Shin H, Ko J, Choi J, Lee H, et al. (2003) Characterization of the movement of the kinesin motor KIF1A in living cultured neurons. J Biol Chem 278: 2624–2629.
47. Babbey CM, Ahktar N, Wang E, Chen CC, Grant BD, et al. (2006) Rab10 regulates membrane transport through early endosomes of polarized Madin-Darby canine kidney cells. Mol Biol Cell 17: 3156–3175.
48. Ullrich O, Reinsch S, Urbe S, Zerial M, Parton RG (1996) Rab11 regulates recycling through the pericentriolar recycling endosome. J Cell Biol 135: 913–924.
49. Ren M, Xu G, Zeng J, De Lemos-Chiarandini C, Adesnik M, et al. (1998) Hydrolysis of GTP on rab11 is required for the direct delivery of transferrin from the pericentriolar recycling compartment to the cell surface but not from sorting endosomes. Proc Natl Acad Sci U S A 95: 6187–6192.
50. Wilcke M, Johannes L, Galli T, Mayau V, Goud B, et al. (2000) Rab11 regulates the compartmentalization of early endosomes required for efficient transport from early endosomes to the trans-golgi network. J Cell Biol 151: 1207–1220.
51. Casanova JE, Wang X, Kumar R, Bhartur SG, Navarre J, et al. (1999) Association of Rab25 and Rab11a with the apical recycling system of polarized Madin-Darby canine kidney cells. Mol Biol Cell 10: 47–61.
52. Wang X, Kumar R, Navarre J, Casanova JE, Goldenring JR (2000) Regulation of vesicle trafficking in madin-darby canine kidney cells by Rab11a and Rab25. J Biol Chem 275: 29138–29146.
53. Zacchi P, Stenmark H, Parton RG, Orioli D, Lim F, et al. (1998) Rab17 regulates membrane trafficking through apical recycling endosomes in polarized epithelial cells. J Cell Biol 140: 1039–1053.
54. Hunziker W, Peters PJ (1998) Rab17 localizes to recycling endosomes and regulates receptor-mediated transcytosis in epithelial cells. J Biol Chem 273: 15734–15741.
55. Drivas GT, Shih A, Coutavas EE, D'Eustachio P, Rush MG (1991) Identification and characterization of a human homolog of the Schizosaccharomyces pombe ras-like gene YPT-3. Oncogene 6: 3–9.
56. Gromov PS, Celis JE, Hansen C, Tommerup N, Gromova I, et al. (1998) Human rab11a: transcription, chromosome mapping and effect on the expression levels of host GTP-binding proteins. FEBS Lett 429: 359–364.
57. Prekeris R, Klumperman J, Scheller RH (2000) A Rab11/Rip11 protein complex regulates apical membrane trafficking via recycling endosomes. Mol Cell 6: 1437–1448.

58. Hales CM, Griner R, Hobdy-Henderson KC, Dorn MC, Hardy D, et al. (2001) Identification and characterization of a family of Rab11-interacting proteins. J Biol Chem 276: 39067–39075.
59. Lindsay AJ, Hendrick AG, Cantalupo G, Senic-Matuglia F, Goud B, et al. (2002) Rab coupling protein (RCP), a novel Rab4 and Rab11 effector protein. J Biol Chem 277: 12190–12199.
60. Wallace DM, Lindsay AJ, Hendrick AG, McCaffrey MW (2002) Rab11-FIP4 interacts with Rab11 in a GTP-dependent manner and its overexpression condenses the Rab11 positive compartment in HeLa cells. Biochem Biophys Res Commun 299: 770–779.
61. Jagoe WN, Lindsay AJ, Read RJ, McCoy AJ, McCaffrey MW, et al. (2006) Crystal structure of rab11 in complex with rab11 family interacting protein 2. Structure 14: 1273–1283.
62. Eathiraj S, Mishra A, Prekeris R, Lambright DG (2006) Structural basis for Rab11-mediated recruitment of FIP3 to recycling endosomes. J Mol Biol 364: 121–135.
63. Shiba T, Koga H, Shin HW, Kawasaki M, Kato R, et al. (2006) Structural basis for Rab11-dependent membrane recruitment of a family of Rab11-interacting protein 3 (FIP3)/Arfophilin-1. Proc Natl Acad Sci U S A 103: 15416–15421.
64. Horgan CP, McCaffrey MW (2009) The dynamic Rab11-FIPs. Biochem Soc Trans 37: 1032–1036.
65. Jing J, Prekeris R (2009) Polarized endocytic transport: the roles of Rab11 and Rab11-FIPs in regulating cell polarity. Histol Histopathol 24: 1171–1180.
66. Horgan CP, Oleksy A, Zhdanov AV, Lall PY, White IJ, et al. (2007) Rab11-FIP3 is critical for the structural integrity of the endosomal recycling compartment. Traffic 8: 414–430.
67. Inoue H, Ha VL, Prekeris R, Randazzo PA (2008) Arf GTPase-activating protein ASAP1 interacts with Rab11 effector FIP3 and regulates pericentrosomal localization of transferrin receptor-positive recycling endosome. Mol Biol Cell 19: 4224–4237.
68. Amorim MJ, Bruce EA, Read EK, Foeglein A, Mahen R, et al. (2011) A Rab11- and microtubule-dependent mechanism for cytoplasmic transport of influenza A virus viral RNA. J Virol 85: 4143–4156.
69. Penfold ME, Armati P, Cunningham AL (1994) Axonal transport of herpes simplex virions to epidermal cells: evidence for a specialized mode of virus transport and assembly. Proc Natl Acad Sci U S A 91: 6529–6533.
70. Lee GE, Murray JW, Wolkoff AW, Wilson DW (2006) Reconstitution of herpes simplex virus microtubule-dependent trafficking in vitro. J Virol 80: 4264–4275.
71. Chambers R, Takimoto T (2010) Trafficking of Sendai virus nucleocapsids is mediated by intracellular vesicles. PLoS One 5: e10994.
72. Deng T, Engelhardt OG, Thomas B, Akoulitchev AV, Brownlee GG, et al. (2006) Role of ran binding protein 5 in nuclear import and assembly of the influenza virus RNA polymerase complex. J Virol 80: 11911–11919.
73. Naito T, Momose F, Kawaguchi A, Nagata K (2007) Involvement of Hsp90 in assembly and nuclear import of influenza virus RNA polymerase subunits. J Virol 81: 1339–1349.
74. Huet S, Avilov SV, Ferbitz L, Daigle N, Cusack S, et al. (2010) Nuclear import and assembly of influenza A virus RNA polymerase studied in live cells by fluorescence cross-correlation spectroscopy. J Virol 84: 1254–1264.
75. Elton D, Simpson-Holley M, Archer K, Medcalf L, Hallam R, et al. (2001) Interaction of the influenza virus nucleoprotein with the cellular CRM1-mediated nuclear export pathway. J Virol 75: 408–419.
76. Torreira E, Schoehn G, Fernandez Y, Jorba N, Ruigrok RW, et al. (2007) Three-dimensional model for the isolated recombinant influenza virus polymerase heterotrimer. Nucleic Acids Res 35: 3774–3783.
77. Resa-Infante P, Recuero-Checa MA, Zamarreno N, Llorca O, Ortin J (2010) Structural and functional characterisation of an influenza virus RNA polymerase-genomic RNA complex. J Virol. pp 11.
78. Hutchinson EC, von Kirchbach JC, Gog JR, Digard P (2009) Genome packaging in influenza A virus. J Gen Virol 91: 313–328.
79. Nakajima K, Ueda M, Sugiura A (1979) Origin of small RNA in von Magnus particles of influenza virus. J Virol 29: 1142–1148.
80. Duhaut SD, McCauley JW (1996) Defective RNAs inhibit the assembly of influenza virus genome segments in a segment-specific manner. Virology 216: 326–337.
81. Odagiri T, Tashiro M (1997) Segment-specific noncoding sequences of the influenza virus genome RNA are involved in the specific competition between defective interfering RNA and its progenitor RNA segment at the virion assembly step. J Virol 71: 2138–2145.
82. Duhaut SD, Dimmock NJ (2002) Defective segment 1 RNAs that interfere with production of infectious influenza A virus require at least 150 nucleotides of 5′ sequence: evidence from a plasmid-driven system. J Gen Virol 83: 403–411.
83. Fujii Y, Goto H, Watanabe T, Yoshida T, Kawaoka Y (2003) Selective incorporation of influenza virus RNA segments into virions. Proc Natl Acad Sci U S A 100: 2002–2007.
84. Noda T, Sagara H, Yen A, Takada A, Kida H, et al. (2006) Architecture of ribonucleoprotein complexes in influenza A virus particles. Nature 439: 490–492.
85. Harris A, Cardone G, Winkler DC, Heymann JB, Brecher M, et al. (2006) Influenza virus pleiomorphy characterized by cryoelectron tomography. Proc Natl Acad Sci U S A 103: 19123–19127.
86. Nayak DP, Hui EK-W, Barman S (2004) Assembly and budding of influenza virus. Virus Research 106: 147–165.
87. Watanabe K, Handa H, Mizumoto K, Nagata K (1996) Mechanism for inhibition of influenza virus RNA polymerase activity by matrix protein. J Virol 70: 241–247.
88. Elster C, Larsen K, Gagnon J, Ruigrok RW, Baudin F (1997) Influenza virus M1 protein binds to RNA through its nuclear localization signal. J Gen Virol 78(Pt 7): 1589–1596.
89. Ye Z, Liu T, Offringa DP, McInnis J, Levandowski RA (1999) Association of influenza virus matrix protein with ribonucleoproteins. J Virol 73: 7467–7473.
90. Cresawn KO, Potter BA, Oztan A, Guerriero CJ, Ihrke G, et al. (2007) Differential involvement of endocytic compartments in the biosynthetic traffic of apical proteins. EMBO J 26: 3737–3748.
91. Rowe RK, Suszko JW, Pekosz A (2008) Roles for the recycling endosome, Rab8, and Rab11 in hantavirus release from epithelial cells. Virology 382: 239–249.
92. Brock SC, Goldenring JR, Crowe JE, Jr. (2003) Apical recycling systems regulate directional budding of respiratory syncytial virus from polarized epithelial cells. Proc Natl Acad Sci U S A 100: 15143–15148.
93. Krzyzaniak MA, Mach M, Britt WJ (2009) HCMV-encoded glycoprotein M (UL100) interacts with Rab11 effector protein FIP4. Traffic 10: 1439–1457.
94. Rossman JS, Jing X, Leser GP, Lamb RA (2010) Influenza virus M2 protein mediates ESCRT-independent membrane scission. Cell 142: 902–913.
95. Abramoff MD, Magelhaes PJ, Ram SJ (2004) Image Processing with ImageJ. Biophotonics International 11: 36–42.
96. Jin M, Goldenring JR (2006) The Rab11-FIP1/RCP gene codes for multiple protein transcripts related to the plasma membrane recycling system. Biochim Biophys Acta 1759: 281–295.

JOURNAL OF INTERFERON & CYTOKINE RESEARCH
Volume 31, Number 11, 2011

DOI: 10.1089/jir.2010.0132

# Interferon-Inducible Antiviral Protein MxA Enhances Cell Death Triggered by Endoplasmic Reticulum Stress

Akiko Numajiri Haruki,* Tadasuke Naito,* Tomomi Nishie, Shoko Saito, and Kyosuke Nagata

Human myxovirus resistance gene A (MxA) is a type I interferon-inducible protein and exhibits the antiviral activity against a variety of RNA viruses, including influenza virus. Previously, we reported that MxA accelerates cell death of influenza virus-infected cells through caspase-dependent and -independent mechanisms. Similar to other viruses, influenza virus infection induces endoplasmic reticulum (ER) stress, which is one of cell death inducers. Here, we have demonstrated that MxA enhances ER stress signaling in cells infected with influenza virus. ER stress-induced events, such as expression of *BiP* mRNA and processing of *XBP1* mRNA, were upregulated in cells expressing MxA by treatment with an ER stress inducer, tunicamycin (TM), as well as influenza virus infection. TM-induced cell death was also accelerated by MxA. Furthermore, we showed that MxA interacts with BiP and overexpression of BiP reduces MxA-promoted ER stress signaling. Because cell death in virus-infected cells is one of ultimate anti-virus mechanisms, we propose that MxA-enhanced ER stress signaling is a part of the antiviral activity of MxA by accelerating cell death.

## Introduction

THE INTERFERON (IFN) SYSTEM plays a central role in host defense against virus infection. IFN-inducible proteins exhibit antiviral roles through translation inhibition, viral RNA metabolism, and so on (García-Sastre and Biron 2006; Sadler and Williams 2008). Furthermore, it was shown that cell death of virus-infected cells, which is one of the ultimate host defense systems, was promoted by some of IFN-inducible proteins, including human myxovirus resistance gene A (MxA) protein (MxA) (Castelli and others 1997; Gil and others 2002; Numajiri and others 2006). MxA is one of the major IFN-inducible proteins and plays a distinct role in the IFN type I-mediated response in cells infected with a variety of viruses such as orthomyxovirus, paramyxovirus, rhabdovirus, togavirus, bunyavirus, coxsackie virus, and hepatitis B virus (Haller and others 2007; Sadler and Williams 2008). A variety of antiviral activities are associated with MxA, although the exact action mechanism is unclear. The anti-viral activity appears to vary depending on the nature of the infecting viruses (Haller and others 2007; Sadler and Williams 2008). MxA may also promote cell death infected with influenza virus (Numajiri and others 2006).

Virus infection causes destruction of infected cells, and induces apoptosis. Most cells undergo cell death while also producing pro-inflammatory cytokines to spread the alarm to their neighboring cells. In turn, viruses employ strategies to regulate the mitochondrial checkpoint for apoptosis, in particular by altering the balance of pro-apoptotic and pro-survival protein levels, by either producing pro-survival inhibitors to lead to cellular death or expressing proteins to maintain cellular survival such as viral Bcl-2 homologs (Galluzzi and others 2008; Postigo and Ferrer 2009).

Several viral proteins have been shown to induce apoptosis through direct effect on mitochondrial compartment or cellular factors. The influenza virus PB1-F2 protein enhances cell death by interaction with ANT3 and VDAC1 proteins at inner and outer mitochondrial membranes, respectively (Zamarin and others 2005). The transforming growth factor-β (TGF-β) activity increases in cells infected with influenza virus. Viral neuraminidase (NA) activates TGF-β, a known inducer of apoptosis, by elimination of sialic acid residues attached to carbohydrates on the latent TGF-β binding protein, which is associated with pro-TGF-β (Schultz-Cherry and Hinshaw 1996; Morris and others 1999). This allows the subsequent removal of the carbohydrate, a pre-determinant for the proteolytic cleavage of pro-TGF-β and release of the active molecule. Viral NS1 and M1 proteins are implicated in modulating apoptotic responses in infected cells. NS1 appears to downregulate apoptosis, although it can induce apoptosis when expressed from a plasmid in absence of virus replication (Morris and others 2002). M1 binds directly with and may inhibit caspase-8 (Zhirnov and others 1999; Timofeeva and others 2001). However, M1 can induce apoptosis in cells expressing this protein from a plasmid. In addition, efficient viral

Department of Infection Biology, Graduate School of Comprehensive Human Sciences, University of Tsukuba, Tsukuba, Japan.
*These two authors contributed to this work equally.

mRNA synthesis has also been shown to be related with apoptosis induction (Stray and Air 2001).

Recently, it was reported that endoplasmic reticulum (ER) stress signaling is triggered and/or regulated by viruses (He 2006). The accumulation of unfolded proteins in the lumen of ER induces a coordinated adaptive program called unfolded protein response (UPR). UPR increases expression of molecular chaperones such as Grp94 and Grp78/BiP to facilitate proper protein folding. Recent studies showed that a variety of viral proteins trigger BiP expression during virus infection, although the effect of upregulation of BiP on virus replication is not fully understood (Jordan and others 2002; Limjindaporn and others 2009). Upon ER stress, activated inositol-requiring enzyme 1 (IRE1) initiates an unconventional splicing of *XBP1* mRNA precursor to excise its unusual intron. The spliced *XBP1* mRNA is efficiently translated into an active basic leucine zipper transcription factor to upregulate transcription of UPR genes (He 2006). Despite of UPR, unfolded proteins often accumulate and can cause apoptosis. C/EBP homologous protein (CHOP), one of the UPR downstream effectors, is a dominant-negative type inhibitor of CCAAT/enhancer-binding proteins. CHOP-mediated apoptosis is known to be coupled with a pathway that suppresses expression of Bcl-2 and intracellular glutathione and the increase of free radicals. The exact downstream target(s) of CHOP remains unclarified (He 2006). It is proposed that IRE1 plays a role in ER stress-mediated apoptosis by the interaction with tumor necrosis factor receptor-associated factor-2, which is thought to be required for the activation of procaspase-12. Activated caspase-12 cleaves procaspase-9 to generate active caspase-9, and consequently leads to activation of the caspase cascade (Urano and others 2000; Rao and others 2002a).

After influenza virus infection, BiP interacts with newly synthesized viral hemagglutinin (HA) and NA proteins (Hurtley and others 1989; Hogue and Nayak 1992). Folding and oligomerization of both proteins are normally efficient, but misfolded HA and NA are generated spontaneously in infected cells, and associate with BiP and then retain in ER. BiP-associated misfolded HA is not transported to the plasma membrane but sustained as complexes in ER for a long period before degradation. These accumulated viral proteins make BiP released from PERK, ATF6, and IRE1, which subsequently activate UPR.

In this study, we have shown that antiviral protein MxA enhances ER stress-mediated cell death after influenza virus infection. Previously, we reported that MxA accelerates cell death induced by influenza viral infection (Mibayashi and others 2002; Numajiri and others 2006). MxA promotes both caspase-dependent and caspase-independent cell death. However, the detailed stimulatory mechanism of cell death induced by MxA is unclear. We found that MxA can enhance transcription of UPR target genes. Furthermore, we have shown that MxA functionally interacts with ER chaperone BiP to promote UPR and apoptosis. Taken altogether, we propose that the cell death promotion activity of MxA plays a role for its antiviral activity.

## Materials and Methods

### Cells, virus infection, and transfection

Swiss mouse 3T3 cell lines, Swiss3T3-Neo and Swiss3T3-MxA cells (Staeheli and others 1986), were kindly provided by Drs. Haller and Kochs and maintained in Dulbecco's modified Eagle's medium supplemented with 10% fetal bovine serum (FBS). HeLa cells were maintained in minimal essential medium supplemented with 10% FBS. All cells were maintained at 37°C in a 5% $CO_2$ incubator. For infection, monolayer cultures of Swiss3T3-Neo and Swiss3T3-MxA cells in 100-mm-diameter dishes were washed twice with serum-free medium, and then infected with influenza A/PR/8 virus at a multiplicity of infection (MOI) of 10 plaque forming unit (PFU) per cell. After virus adsorption at 37°C for 1 h, the cells were washed with serum free medium and then incubated with the fresh medium at 37°C for indicated periods. Transfection of HeLa and HEK293T cells with plasmids was carried out by the standard calcium phosphate method or using transfection reagent TransIT (Mirus).

### Chemical compounds

Tunicamycin (TM) and salubrinal (Sal) were purchased from Calbiochem. Brefeldin A (BFA) was purchased from Wako. These compounds were dissolved in dimethlysulfoxide.

### Construction of plasmid vectors

An eukaryotic expression vector, pCHA-MxA, was constructed previously (Mibayashi and others 2002). To construct pCHA-MxA mutant vectors, pCHA-MxAΔC241 and pCHA-MxAΔC574, the insert cDNAs were amplified by polymerase chain reaction (PCR), digested with *Mlu*I and *Afl*II, and subloned into *Mlu*I- and *Afl*II-digested pCHA vector. PCR amplification was performed using pCHA-MxA as template and primers as follows: 5′-GGACGCGTATGGTTGTTTCCGAA GTGGAC-3′ for pCHA-MxAΔC241 and pCHA-MxAΔC574, 5′-GGCTTAAGTCATTAGACCACCACCAGGCTGAT-3′ for pCHA-MxAΔC241, and 5′-GGCTTAAGTCATTAGGAAGA GTCTGTTGCCGA-3′ for pCHA-MxAΔC574. Plasmids of pCHA-MxAΔC and pCHA-MxAΔN were prepared as described previously (Numajiri and others 2006).

Plasmid vectors for luciferase assays, pGL3-GRP78P(-132)-luc (Yoshida and others 1998) and p5xATF6GL3 (Wang and others 2000) designated ER stress response element (ERSE) and UPR element (UPRE) reporters, respectively, were kind gifts from Drs. Mori and Prywes, respectively. For construction of mammalian expression vector for mouse BiP, a cDNA fragments corresponding to BiP ORF with a FLAG tag at its N-terminus was amplified by reverse transcriptase (RT)-PCR with primers 5′ GCGGATCCCCGCCACCATG ACTACAAGGATGACGACAAGATGATGAAGTTCACTG TGGTGGC 3′ and 5′ GCGGATCCCTACAACTCATCTTT TTCTGATGTATC 3′ and mouse total RNA as template. PCR product was digested with *Bam*HI (TOYOBO), and inserted into the *Bam*HI site of pcDNA3 (Invitrogen) to create pcDNA3-FLAG-BiP. The details for the generation of the plasmid for hNAP-1 (Okuwaki and others 2010) will be described elsewhere.

### Reverse transcriptase–polymerase chain reaction

Total RNA was isolated from Swiss3T3-Neo and Swiss3T3-MxA cells by the guanidine method. cDNA was synthesized from total RNA (0.5–2 μg) using Superscript II reverse transcriptase (RT; Invitrogen) and oligo-$dT_{20}$ primer. PCR was performed using the above cDNAs (1/20, vol/vol) as template and a set of specific primers by pre-determined

PCR cycles, under which PCR products are semi-logarithmically amplified. Primer sequences used in this study were as follows: for mouse (m) *BiP*, 5′ AAGGTCTATGAAGGTG AACGACCCC 3′ and 5′ GACCCCAAGACATGTGAGCA ACTGC 3′; for m*XBP1*, 5′ CACGCTTGGGAATGGACACG 3′ and 5′ GATGAGGTCCCCACTGACAG 3′; for m*CHOP*, 5′ GCACGCGTATGGCAGCTGAGTCCCTGC 3′ and 5′ GCG ATATCATGCTTGGTGCAGGCTGA 3′; and for m*β-actin*, 5′ ATGGGTCAGAAGGACTCCTATGTGGG 3′ and 5′ CTAG AAGCACTTGCGGTGCACGATG 3′. The PCR products were separated on 1% agarose gel electrophoresis for *BiP*, *CHOP*, and *β-actin*, and 8% polyacrylamide gel electrophoresis (PAGE) for *XBP1*, and observed by staining with EtBr.

### Real-time RT-PCR

Total RNA extraction was performed with RNeasy minikit (Qiagen), and reverse-transcribed into cDNAs by using a ReverTra Ace and oligo(dT) primer (TOYOBO). The amounts of cDNAs for *CHOP* and *β-actin* were quantified using Fast Start SYBR Green Master (Roche).

### Trypan blue dye exclusion assay

Typan blue dye exclusion assays were carried out as previously described (Numajiri and others 2006). Swiss3T3-Neo and Swiss3T3-MxA cells in 60-mm-diameter dishes were treated with TM (SIGMA). After cell death induction for indicated periods, both adherent and floating cells were collected together by centrifugation. The cells were resuspend in 0.02% trypan blue (SIGMA) in phosphate-buffered saline (PBS), and dead and living cells were counted using hemocytometer.

### Fluorescence-activated cell sorter analysis

Cells were treated as indicated in figure legends, collected, and then stained with propidium iodide (5 μg/mL). Fluorescence-activated cell sorting (FACS) analysis was performed using FACSCalibur instrument (BD biosciences) using CellQuest software.

### Luciferase assay

The luciferase activity was determined using commercially available reagents (Promega) according to the manufacturer's protocol. The relative luciferase activity was measured for 10 s with a luminometer. The *Firefly* luciferase activity was normalized as that relative to the *Renilla* luciferase activity derived from a co-transfected control plasmid pRL-SV40 (Promega).

### Indirect immunofluorescence assay

The double immunostaining of HA-MxA, FLAG-BiP, and PB1 was carried out at room temperature as follows: HeLa cells grown on glass coverslips in culture dishes were transfected with plasmid DNAs. After 24 h post transfection, the cells were infected with influenza A/PR/8 virus at MOI of 10 PFU per cell according to the protocol described above. After 8 h postinfection (hpi), cells were washed, fixed with PBS containing 4% paraformaldehyde, and then permeabilized with PBS containing 0.5% Triton X-100. The coverslips were soaked in TBS-T [25 mM Tris-HCl (pH 7.9), 137 mM NaCl, and 3 mM KCl, 0.1% Tween 20] containing 5% skim milk for 30 min. Cells were then incubated for 1 h with primary antibodies: mouse anti-HA clone 12CA5 (1:250; Roche), rat anti-HA clone 3F10 (1:3,000; Roche), rabbit anti-PB1 antibodies (1:500) (Naito and others 2007), or mouse anti-FLAG M2 (1:3,000; SIGMA) monoclonal antibodies. After washing with PBS containing 0.1% NP-40, the cells were incubated for 30 min with secondary antibodies: Alexa Fluor 488 goat anti-mouse (1:2,000; Molecular Probe, A11029), Alexa Fluor 568 goat anti-rabbit (1:2,000; Molecular Probe, A11011), and Alexa Fluor 633 goat anti-rat (1:2,000; Molecular Probe, A21094) antibodies. Coverslips were washed with PBS containing 0.1% NP-40, and incubated for 10 min with 10 mM 4′,6′-diamido-2-phenylindole dihydrochloride. After washing with PBS containing 0.1% NP-40, the coverslips were mounted on slide glasses. The cells were then observed under a fluorescence microscope (Carl Zeiss).

### Immunoprecipitation assays

Transfected cells were washed with PBS and collected by centrifugation. Cells were re-suspended in IP buffer [20 mM Tris-HCl (pH 7.9), 150 mM NaCl, 30 mM KCl, 1 mM EDTA, and 0.1% NP-40]. After sonication, homogenates were centrifuged at 10,000 rpm at 4°C for 10 min. The supernatant was recovered and used for immunoprecipitation assays. Cell extracts were mixed with mouse anti-MxA KM1124 (Kyowa Medex) or mouse anti-FLAG M2 (SIGMA) antibodies and incubated at 4°C for 2 h. Immunocomplexes were recovered by the addition of protein A Sepharose Fast Flow beads (GE Healthcare). The beads were washed 3 times with IP buffer. Immunoprecipitated proteins were separated by sodium dodecyl sulfate–10% PAGE and subjected to western blot analyses using anti-HA clone 3F10 and anti-FLAG M2 antibodies.

## Results

### ER stress-mediated cell death is promoted by MxA

Previously, we reported that MxA has the cell death promotion activity (Mibayashi and others 2002; Numajiri and others 2006). After influenza virus infection, cells expressing MxA died faster than MxA-negative cells. Here, we have addressed how the cell death, after influenza virus infection, is triggered in cells expressing MxA. It is well established that one of the triggers of the cell death upon viral infection is the ER stress-induced cell death mechanism (He 2006). Indeed, *BiP* mRNA accumulates after influenza virus infection (Maruoka and others 2003). Thus, we first examined the expression level of *BiP* mRNA in cells expressing MxA upon influenza virus infection. In this study, we used Swiss3T3-MxA, a previously established cell line expressing MxA constitutively (Staeheli and others 1986), because MxA is IFN-inducible in certain cells and the addition of IFN may affect other IFN-related cell death/survival pathways. The level of *BiP* mRNA was upregulated in cells expressing MxA at 3 hpi (Fig. 1A). In addition, splicing of *XBP1* mRNA, an event closely correlated with ER stress, was also enhanced in cells expressing MxA at 3 hpi. These results showed that MxA enhances ER-mediated stress signaling after influenza virus infection.

Next, we examined whether MxA enhances ER stress-mediated stress signaling leading to cell death promotion upon stimuli other than influenza virus infection, because

influenza virus infection may induce a variety of cellular signaling pathways. We utilized an ER stress inducer, TM, which inhibits N-linked glycosylation and thereby causes protein accumulation in ER. Swiss3T3-MxA and Swiss3T3-Neo cells negative in MxA expression were treated with 0.5 μg/mL of TM, and then subjected to trypan blue dye exclusion assays. While TM induces cell death in both MxA-positive and control cells, the number of dead cells was 8–10 times greater in MxA-positive cells (Fig. 1B). More than 70% of MxA-positive cells died at 48 h after TM treatment.

In parallel, we examined whether caspase-12 activation is further enhanced by MxA. Caspase-12 is activated specifically in cells suffered from ER stress (Morishima and others 2002) and functions as the initiator caspase in response to a toxic insult to ER, such as treatment with TM or calcium ionophores (Nakagawa and others 2000). Treatment of cells with TM resulted in the processing of procaspase-12 (48 kDa) (Fig. 1C). We found that the procaspase-12 level decreased, whereas one of cleaved products increased. We could not detect the prodomain, because caspase-12 antibody used (SIGMA; C7611) here does not recognize the prodomain. Key finding is that the cleavage of procaspase-12 was enhanced in MxA-positive cells upon TM treatment. This result suggests that MxA promotes ER stress-mediated cell death after TM treatment.

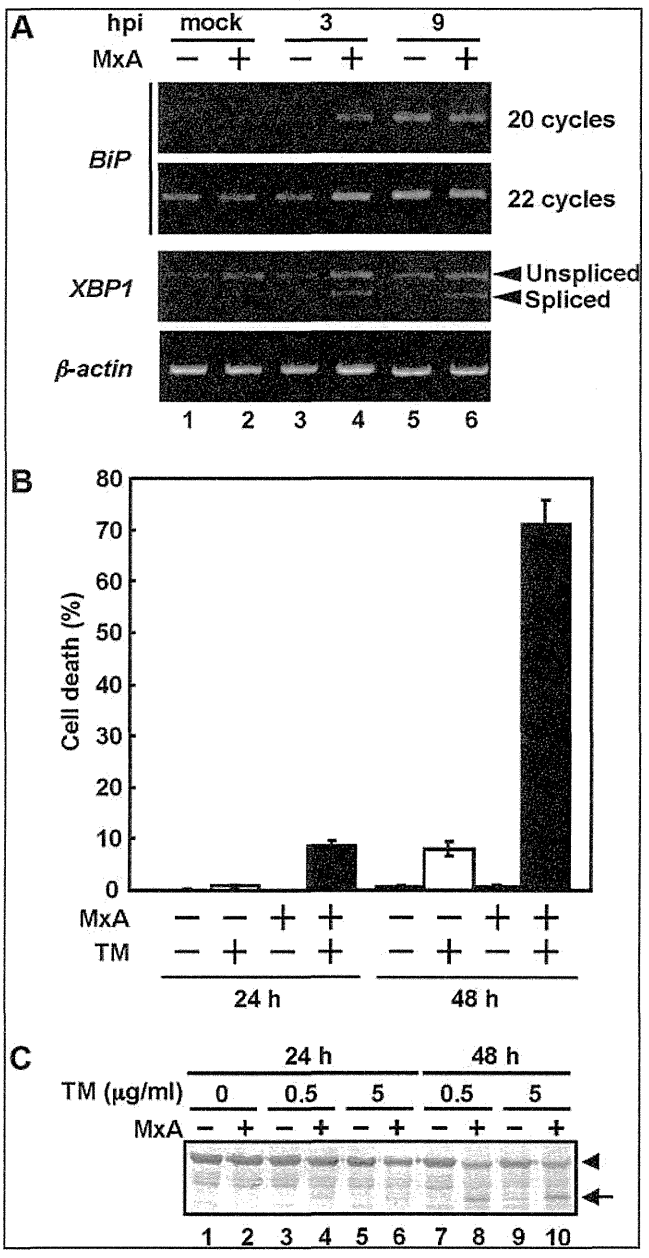


### *Promotion of apoptosis mediated by MxA is repressed in the presence of a selective inhibitor of ER stress response*

MxA was involved in apoptosis acceleration induced by TM (Fig. 1B, C). However, a rapid accumulation of proteins within ER and collapse of Golgi stacks by treatment of TM or BFA may induce various apoptosis pathways beside ER stress-induced cell death. We examined whether MxA specifically functions in UPR-mediated apoptosis by using a selective inhibitor, Sal. Sal blocks dephosphorylation of eukaryotic translation initiation factor 2 subunit α and protects cells from ER stress-induced apoptosis (Boyce and others 2005).

To determine the effect of Sal on ER stress pathway-specific apoptosis acceleration by MxA, we carried out FACS analyses. As shown in Fig. 2A, we confirmed using the FACS method that cell death is induced by TM treatment and further promoted by MxA. Previously, we showed that cell death is enhanced in MxA-expressing cells when cells were treated with cycloheximide (CHX) or ultraviolet irradiation (Numajiri and others 2006). In this report, we examined the impact of Sal on BFA-induced stress condition (Fig. 2B). Cell death was induced by BFA, and enhanced in cells expressing of MxA. Sal suppressed BFA-induced apoptosis, to some extent, not only in MxA-negative cells, but also in MxA-positive cells. These results suggest that apoptosis acceleration by MxA, at least in part, is caused through ER stress signal pathway.

**FIG. 1.** Cell death is stimulated by TM in cells expressing MxA. **(A)** MxA enhances ER stress caused by influenza virus. Swiss3T3-Neo and Swiss3T3-MxA cells were infected with influenza virus at MOI of 10. After incubation for 3 and 9 h, cells were collected, and the DNA fragment corresponding to *BiP* mRNA was amplified from total RNA by RT-PCR. Resulting products were subjected to 1% agarose gel electrophoresis for *BiP* mRNA (*upper 2 panels*) and *β-actin* mRNA (*lower*) or 8% PAGE for *XBP1* mRNA (*middle*). Unspliced and spliced forms of *XBP1* mRNA were indicated by *arrowheads*. **(B)** Dye exclusion assay. Swiss3T3-Neo (*open columns*) and Swiss3T3-MxA (*filled columns*) cells were treated with TM (0.5 μg/mL). After incubation for 24 and 48 h under cell death induction, cells were collected and subjected to trypan blue dye exclusion assays. **(C)** Cleavage of procaspase-12 upon TM treatment. Swiss3T3-Neo and Swiss3T3-MxA cells were treated with TM (0.5 or 5 μg/mL). After incubation for 24 and 48 h under cell death induction, cells were collected and subjected to western blot analyses with anti-caspase-12 antibody (SIGMA). Procaspase-12 and cleaved forms were indicated by *arrowhead* and *arrow*, respectively. TM, tunicamycin; ER, endoplasmic reticulum; MOI, multiplicity of infection; RT-PCR, reverse transcriptase–polymerase chain reaction.

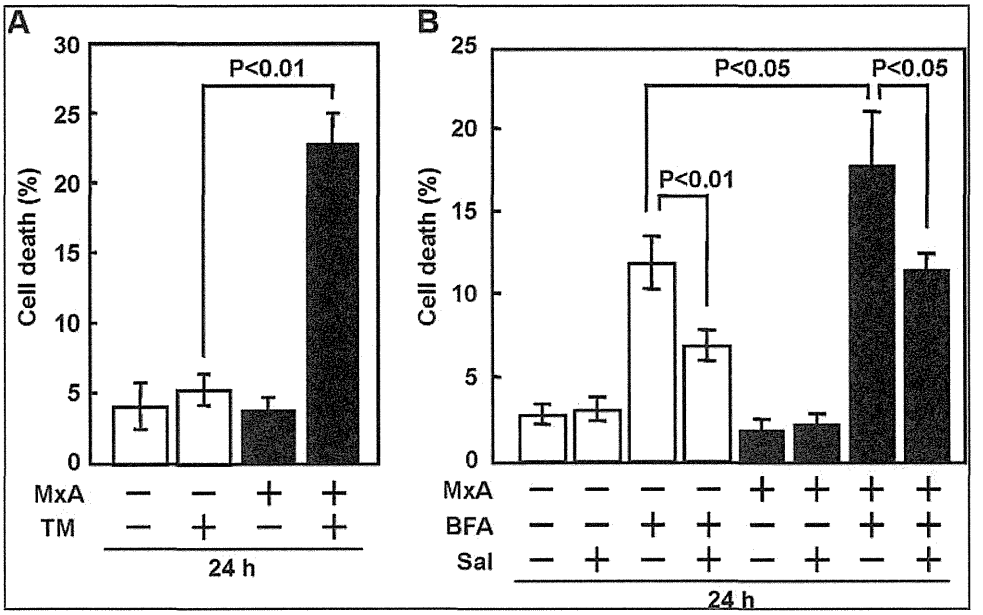


FIG. 2. Sal, a selective ER stress inhibitor suppresses apoptosis accelerated by MxA. **(A)** Swiss3T3-Neo (*open columns*) and Swiss3T3-MxA (*filled columns*) cells were treated with TM (0.5 μg/mL). After incubation for 24 h, cells were collected and subjected to FACS analysis. **(B)** Effect of Sal on MxA-induced cell death. Swiss3T3-Neo (*open columns*) and Swiss3T3-MxA (*filled columns*) cells were treated with 50 μM BFA in the presence or absence of 15 μM Sal. After incubation for 24 h, cells were collected and subjected to FACS analysis. Data were presented as means with standard deviation from 3 independent experiments. FACS, fluorescence-activated cell sorting; BFA, Brefeldin A; Sal, Salubrinal.

### *MxA accelerates UPR after TM treatment*

We next examined whether UPR signaling induced by TM is also enhanced in cells expressing MxA. To this end, we examined the mRNA expression level of genes under the control of the UPR signaling. Swiss3T3-MxA and Swiss3T3-Neo cells were treated with TM, and the mRNA level was examined by RT-PCR method. After 6 and 3 h in the presence of 0.5 and 2.5 μg/mL TM, respectively, the *BiP* mRNA level was increased in cells expressing MxA (Fig. 3A, compare lane 5 with lane 6, and lane 7 with lane 8). From 3 h after treatment with 0.5 μg/mL TM, the spliced form of *XBP1* mRNA was detected in cells expressing MxA, whereas this occurred from 12 h after treatment with TM in MxA-negative cells (Fig. 3B). One of the known signals coordinated with ER stress-induced apoptosis is the expression of CHOP (He 2006). As shown in Fig. 3C, after the treatment with 0.5 μg/mL TM, only MxA-positive cells expressed *CHOP* mRNA. Increase of mRNA amount of the gene under the control of the UPR pathway was distinct only in the presence of low concentrations of TM (Fig. 3C, lanes 4 and 6). This MxA-mediated enhancement was not observed when cells were treated with 2.5 μg/mL TM. MxA may not affect ER signaling induced by vast amounts of unfolded proteins. Furthermore, we confirmed that the amount of *CHOP* mRNA is upregulated in cells transiently expressing MxA (Fig. 3D). Collectively, these suggest that MxA reduces the threshold level of ER stress sensing.

We determined whether MxA enhances the transcription promoter activity directed by ERSE or UPRE under the control of UPR. We utilized pGL3-GRP78P(-132)-luc and p5xATF6GL3 plasmids to monitor ERSE- and UPRE-dependent promoter activities, respectively (Zhu and others 1997; Yoshida and others 1998; Wang and others 2000). As shown in Fig. 3E, F, MxA enhanced both ERSE- and UPRE-dependent promoter activities in response to TM treatment. This enhancement by MxA was in a dose-dependent manner and was undetectable when a reporter plasmid pGL3-GRP78Pmut that lacks ERSE was used (data not shown). These results suggest that MxA affects the signaling pathway leading to the transcription activation upon ER stress response or UPR.

### *MxA interacts with BiP*

We showed that MxA enhances both ATF6- and IRE1-dependent activation of ER stress responses. BiP, an ER chaperone, is known to bind to and stabilize these ER stress sensors (He 2006). Therefore, we consider the possibility that MxA interacts with BiP, either directly or indirectly, and depletes this chaperone in the ER stress response. Since majorities of BiP are localized inside of ER, while MxA is in the cytoplasm, we assumed that an additional factor(s) is involved in the BiP and MxA interaction. However, it is reported that some of BiP is also localized in the cytoplasm (Buchkovich and others 2009). In fact, cytoplasmic BiP interacts with caspase-7 and caspase-12 to prevent cell death (Rao and others 2002b).

As shown in Fig. 4A, MxA and BiP were co-localized around ER in cells co-expressing both proteins. Furthermore, the localization pattern of MxA and BiP in uninfected cells was similar to that observed in influenza virus-infected cells (compare with Fig. 4A, B). At 9 hpi, PB1 was present in the nucleus and the cytoplasm (Fig. 4B). In the same cell, MxA and BiP were co-localized in ER and cytoplasm.

To examine whether MxA interacts with BiP *in vivo*, we performed immunoprecipitation assays using lysates prepared from cells transfected with expression plasmids for FLAG-BiP and either HA-MxA wild type (wt) or mutants (Fig. 4C). Western blot analyses revealed that HA-MxAwt was co-immunoprecipitated with FLAG-BiP when anti-FLAG antibody was used (Fig. 4C, lane 10). We used human nucleosome assembly protein-1-L1 (hNAP-1), one of cytoplasmic proteins, as negative control for overexpression condition (Fig. 4C, lanes 1 and 8). In addition, we tried to identify an interaction domain on MxA and binding specificity with BiP. MxAΔC574 lacking zinc finger motif bound to BiP but only weakly, and MxAΔN interacted with BiP a

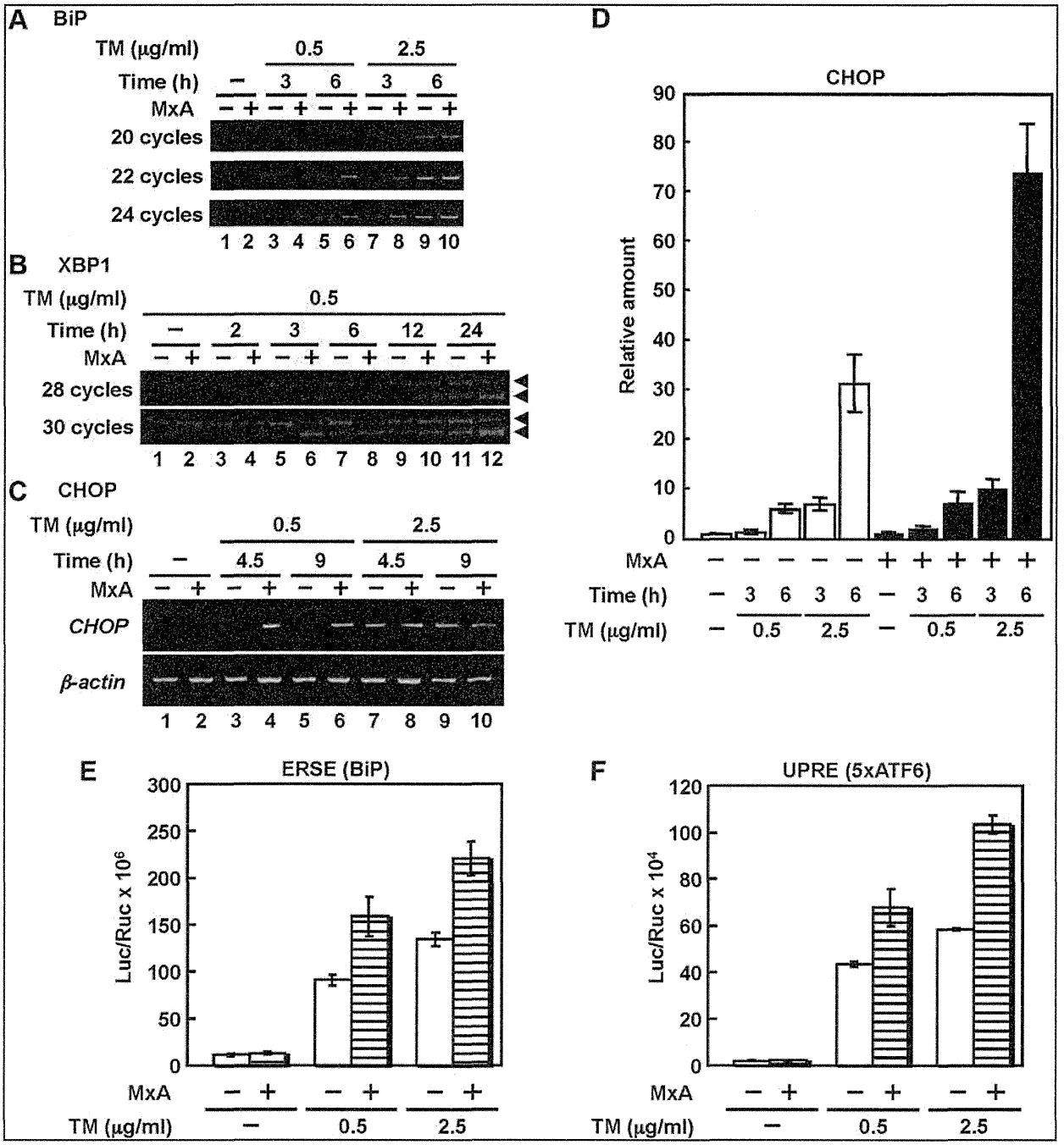


**FIG. 3.** MxA accelerates UPR after TM treatment. **(A–C)** Swiss3T3-Neo and Swiss3T3-MxA cells were treated with TM at the indicated concentration. After incubation for indicated time periods, cells were collected, and total RNA were subjected to RT-PCR. Amplified DNA fragments were subjected to separation on 1% agarose gel electrophoresis for *BiP* mRNA **(A)** and *CHOP* mRNA **(C)**, or 8% PAGE for *XBP1* mRNA **(B)**. Unspliced and spliced forms of *XBP1* mRNA were indicated by *arrowheads*. **(D)** Quantification of *CHOP* mRNA in MxA-transfected cells using real-time RT-PCR. Swiss3T3 cells were transfected with pCHA or pCHA-MxA plasmid with pBabe-puro. At 24 h post transfection, 2 μg/mL puromycin was added, and cells were grown for further 24 h in growth medium in the presence of 2 μg/mL puromycin. Puromycin-resistant cells were treated with TM at indicated concentrations for 3 and 6 h. **(E, F)** MxA enhances both ERSE and UPRE. HeLa cells were transfected with pGL3-GRP78P(-132)-luc or p5xATF6GL3 in the presence (*striped columns*) or absence (*open columns*) of an expression plasmid encoding MxA, pCHA-MxA (Mibayashi and others 2002). pRL-SV40 encoding the *Renilla* luciferase was used for internal control. At 24 h after transfection, the cells were treated with or without TM (0.5 or 2.5 μg/mL) for 12 h, and *Firefly* and *Renilla* luciferase activities were measured. The *Firefly* result was normalized by the *Renilla* luciferase activity. UPR, unfolded protein response; ERSE, ER stress response element; UPRE, UPR element.

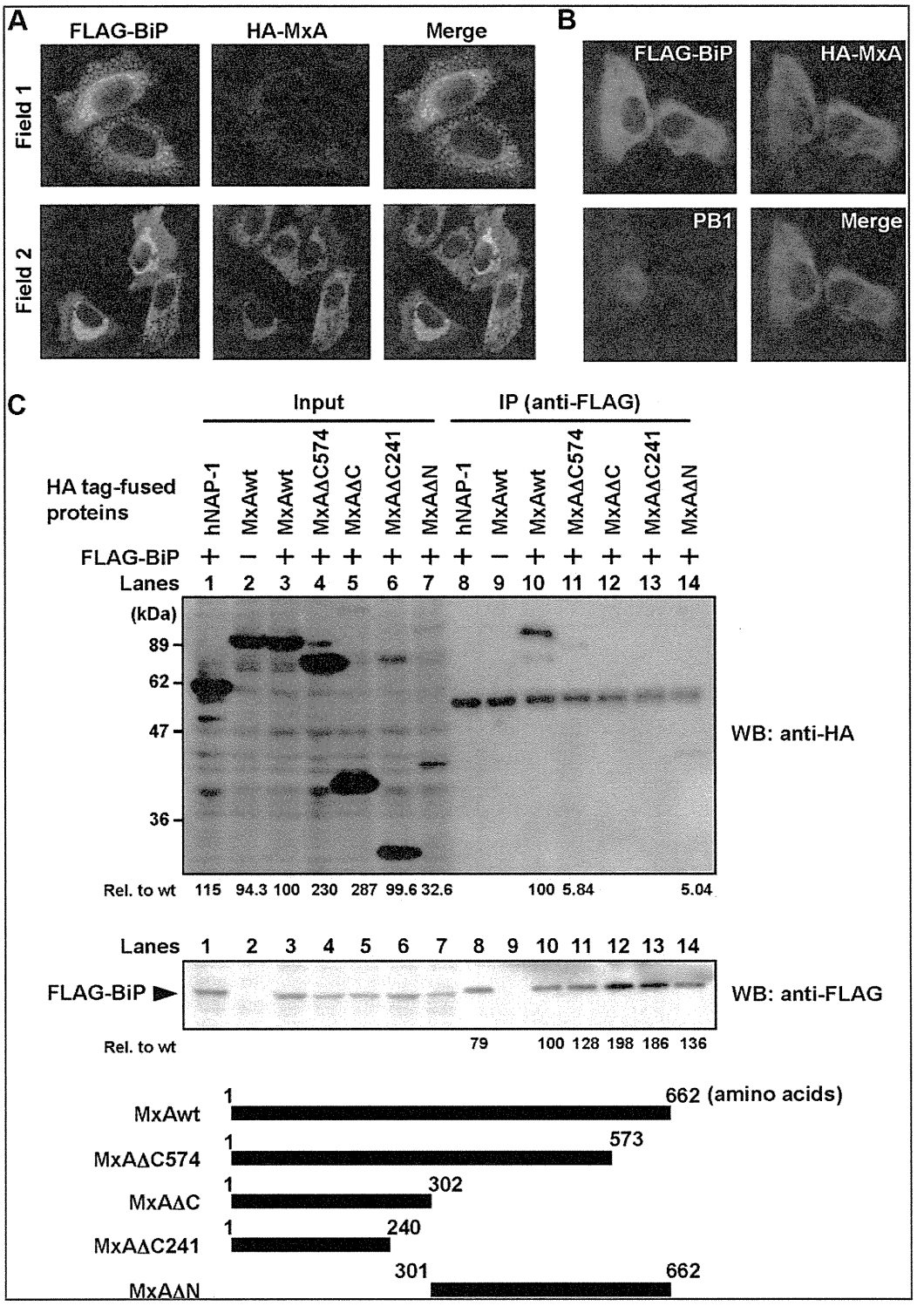


**FIG. 4.** MxA interacts with BiP. **(A)** Fluorescent immunocytochemical analysis. HeLa cells were transfected with pcDNA-FLAG-BiP and pCHA-MxA, and double-stained with both anti-FLAG and anti-HA antibodies. **(B)** Fluorescent immunocytochemical analysis. HeLa cells were co-transfected with pcDNA3-FLAG-BiP and pCHA-MxA, and at 1 day after transfection, cells were infected with influenza virus at MOI of 10. After incubation for 9 h, cells were collected, and stained with anti-FLAG, anti-HA, and anti-PB1 antibodies. **(C)** Immunoprecipiation assays. HEK293T cells were transfected with pCHA-hNAP-1 (lane 1) or pCHA-MxA mutants (lanes 2–7) in the presence (lanes 1, 3–7) or absence (lane 2) of pcDNA3-FLAG-BiP. Cells were collected at 1 day after transfection, and lysates were subjected to immunoprecipitation assays using anti-FLAG antibody (lanes 8–14). Immunoprecipitated proteins were examined by western blot analyses with anti-HA (*upper panel*) and anti-FLAG antibodies (*lower panel*). Detected protein levels are indicated at the bottom as values relative to those seen in lanes 3 and 10 for the input amount and the immunoprcipitated amount, respectively. MxA mutants used in this assay are schematically illustrated.

little more than MxAΔC574 when compared with the input amounts. However, deletion mutants in the C terminal region, MxAΔC or MxAΔC241 (Fig. 4C, lanes 11 to 14), had virtually no binding capability. Thus, it is quite likely that the region between amino acid positions 301 to 573 of MxA is essential for the binding to BiP. These results indicate that MxA and BiP form a complex around ER. We speculate that this interaction could lead to the activation of ER stress response or the UPR.

### *BiP suppresses UPR promotion activity of MxA*

Finally, we examined whether overexpression of BiP could suppress the ER stress enhancement activity of MxA. We reasoned that either indirect or direct binding of MxA to BiP could be rescued by overexpression of BiP. Reporter gene assays were performed with exogenously overexpressed BiP. Fig. 5A shows that the ER stress response in the absence of TM is not affected by the overexpression of FLAG-BiP. In contrast, in the presence of TM, the activation of ER stress response by MxA was cancelled by overexpressed FLAG-BiP in a dose-dependent manner. Fig. 5B confirmed the expression level of HA-MxA and FLAG-BiP. Thus, it seems likely that ER stress chaperone BiP

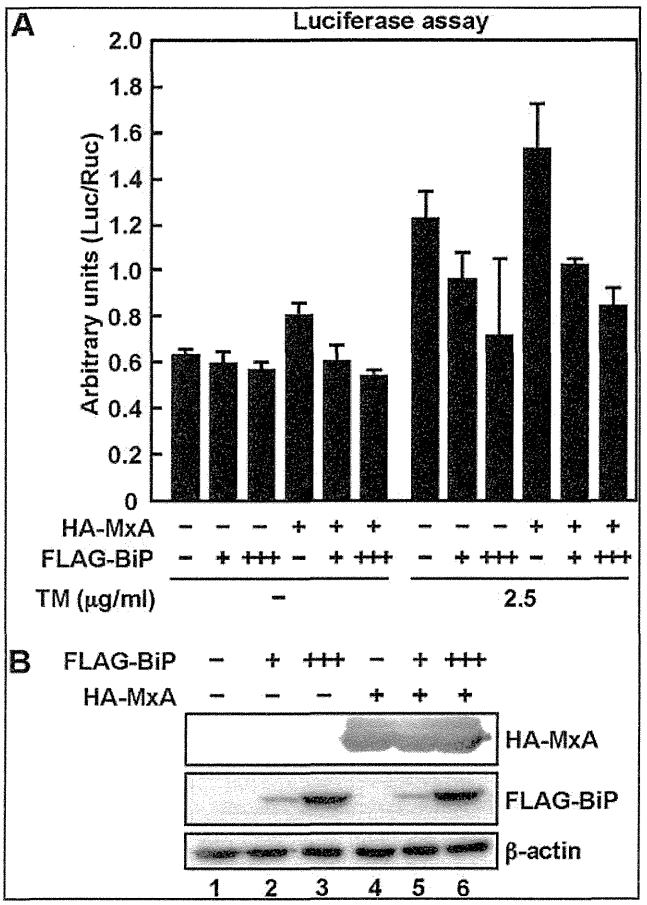


**FIG. 5.** BiP cancelled UPR promotion activity of MxA. **(A)** Reporter gene assay. HeLa cells were transfected with the reporter plasmid pGL3-GRP78P(-132)-luc with or without pCHA-MxA and pcDNA-FLAG-BiP as described in the figure. At 15 h post transfection, the cells were treated with or without TM (2.5 μg/mL) for 12 h, and the luciferase activity was measured. **(B)** Western blot analyses. Cells treated with TM as shown in **(A)** were subjected to western blot analyses with anti-HA (*upper*), anti-FLAG (*middle*), or anti-β-actin antibodies (*lower*).

cannot be used for its proper role by its depletion through the binding to MxA, either directly or indirectly, on ER membrane. This may reduce the threshold level of ER stress sensing, and thereby promotes the ER stress-induced apoptosis.

## Discussion

MxA is an IFN-induced 76 kDa-GTPase that inhibits the multiplication of a variety of RNA viruses, although the exact mechanism of the MxA action is unclear. The antivirus mechanism seems to vary depending on infecting viruses (Schnorr and others 1993; Schneider-Schaulies and others 1994; Landis and others 1998; Gordien and others 2001). When cells expressing MxA are infected with influenza virus, the primary transcription catalyzed by virion-associated viral RNA polymerases occurs at the same level as that in MxA-negative cells (Pavlovic and others 1992). In contrast, viral protein synthesis and genome replication are strongly inhibited (Pavlovic and others 1992). If MxA is forced to be present in the nucleus, nuclear MxA can suppress the influenza virus transcription by interacting with not only the viral polymerase subunit PB2, but also with NP (Turan and others 2004). In addition, we reported that MxA has the cell death promotion activity (Mibayashi and others 2002; Numajiri and others 2006). After influenza virus infection, MxA-positive cells dies faster than MxA-negative cells. We have also shown the caspase-dependent and -independent cell death promotion activity by MxA. It has been reported that the activation of caspase-3 is important during influenza virus proliferation (Queitsch and others 2002). However, the activation level of caspase-3 did not differ between MxA-expressing and MxA-negative cells (Numajiri and others 2006). Therefore, it is possible that MxA could promote cell death without elevation of influenza virus production.

Influenza viruses cause cell death by several mechanisms (Ludwig and others 2006; Sanders and others 2011). Virus infection can induce cell lysis directly, which releases progeny virions and accumulation of a large amount of viral proteins together with potential inflammatory. Promotion of cell death in virus-infected cells may lead to suppression of progeny virion production. The induction of apoptosis might be mediated via intrinsic and/or extrinsic mechanism. It has been shown that viral activation of mitogen-activated protein kinases or their upstream kinases is linked to the onset of apoptosis, and virus infection results in an activation of nuclear factor-κB as an intrinsic pathway. On the other hand, as an extrinsic mechanism of viral apoptosis induction, it has been indicated that the Fas/FasL apoptosis pathway undergoes in a double-stranded RNA activated protein kinase (PKR)-dependent manner in infected cells. The mechanism of viral apoptosis induction might occur via activation of TGF-β, a known apoptosis inducer that is converted from its latent form by NA.

Here, we have addressed the question how MxA promotes cell death after influenza virus infection in light of ER stress signaling. Recent reports suggest that some viruses cause and/or regulate ER stress (Bitko and Barik 2001; Su and others 2002; Tardif and others 2002, 2004; Medigeshi and others 2007). For example, human cytomegalovirus (HCMV) induces splicing of *XBP1* transcript, whereas HCMV suppresses the expression of genes normally regulated by XBP1. It is possible that HCMV utilizes a part of UPR and prevents cell death simultaneously (Isler and others 2005). Dengue

virus envelope protein interacts with BiP and facilitates proper protein folding and protein assembly required for production of progeny virus particles (Limjindaporn and others 2009). In this report, we have shown that MxA enhances ER stress signaling and ER stress-induced cell death upon influenza virus infection. MxA upregulated the transcription level of *BiP* mRNA and the splicing of *XBP1*. MxA also upregulated the transcription level of *CHOP* gene, which is known to be a key mediator for ER stress-induced cell death. Consistent with our findings, CHOP-dependent premature cell death may represent a host defense mechanism to limit viral replication (Medigeshi and others 2007). Previously, we reported that the cell death promotion activity was detected for both MxAwt and MxAΔN, but not for MxΔC in cells treated with CHX as stress inducer. Here, we have shown that the C terminal region on MxA containing oligomelization domain was important in the interaction with BiP. Therefore, similar to the promotion of CHX-induced cell death by MxA, MxA may function as apoptosis accelerator for ER stress-mediated cell death through the same C terminal region.

Previous studies demonstrated that a portion of MxA is localized at membranes belonging to the COP-I-positive subdomain of the smooth ER-Golgi-intermediate compartment (Accola and others 2002; Stertz and others 2006). Furthermore, it has been reported that binding of MxA to viral nucleocapsid protein of La Crosse virus occurs on membranes of the smooth ER-Golgi boundary region and lead to a depletion of the nucleocapsid protein from the viral replication sites (Kochs and others 2002). However, it is presently not clear how MxA interacts with lipid membranes. Anchoring of MxA to distinct membrane compartments may influence the antiviral activity and/or specificity. Recently, Gao and others (2010) reported that the crystal structure of oligomerized stalk region of MxA, which is composed of the middle domain and the GTPase effector domain. The MxA could form a linear oligomers comprised of 13 to 14 dimers. It is not clear how a huge complex of MxA formed through this structure is associated with or incorporated into intracellular membranes. Further studies are needed to clarify details of the connection of MxA-mediated ER stress promotion with antiviral activity.

## Acknowledgments

We thank Drs. O. Haller and P. Staeheli (University of Freiburg, Freiburg, Germany), K. Mori (Kyoto University, Kyoto, Japan), and R. Prywes (Columbia University, New York) for their generous gifts of Swiss3T3 and Swiss3T3-MxA cells, and MxA wild-type cDNA, pGL3-GRP78P(-132)-luc, and p5xATF6GL3, respectively. We also thank Dr. Kiong Ho for proofreading the article. This work was supported in part by grants-in-aid from the Ministry of Education, Culture, Sports, Science, and Technology of Japan (T.N. and K.N.).

## Author Disclosure Statement

No competing financial interests exist.

## References

Accola M, Huang B, Al Masri A, McNiven M. 2002. The antiviral dynamin family member, MxA, tubulates lipids and localizes to the smooth endoplasmic reticulum. J Biol Chem 277:21829–21835.

Bitko V, Barik S. 2001. An endoplasmic reticulum-specific stress-activated caspase (caspase-12) is implicated in the apoptosis of A549 epithelial cells by respiratory syncytial virus. J Cell Biochem 80:441–454.

Boyce M, Bryant KF, Jousse C, Long K, Harding HP, Scheuner D, Kaufman RJ, Ma D, Coen DM, Ron D, Yuan J. 2005. A selective inhibitor of eIF2alpha dephosphorylation protects cells from ER stress. Science 307:935–939.

Buchkovich N, Maguire T, Paton A, Paton J, Alwine J. 2009. The endoplasmic reticulum chaperone BiP/GRP78 is important in the structure and function of the human cytomegalovirus assembly compartment. J Virol 83:11421–11428.

Castelli J, Hassel B, Wood K, Li X, Amemiya K, Dalakas M, Torrence P, Youle R. 1997. A study of the interferon antiviral mechanism: apoptosis activation by the 2-5A system. J Exp Med 186:967–972.

Galluzzi L, Brenner C, Morselli E, Touat Z, Kroemer G. 2008. Viral control of mitochondrial apoptosis. PLoS Pathog 4, e1000018.

Gao S, von der Malsburg A, Paeschke S, Behlke J, Haller O, Kochs G, Daumke O. 2010. Structural basis of oligomerization in the stalk region of dynamin-like MxA. Nature 465:502–506.

García-Sastre A, Biron C. 2006. Type 1 interferons and the virus-host relationship: a lesson in détente. Science 312:879–882.

Gil J, García M, Esteban M. 2002. Caspase 9 activation by the dsRNA-dependent protein kinase, PKR: molecular mechanism and relevance. FEBS Lett 529:249–255.

Gordien E, Rosmorduc O, Peltekian C, Garreau F, Bréchot C, Kremsdorf D. 2001. Inhibition of hepatitis B virus replication by the interferon-inducible MxA protein. J Virol 75:2684–2691.

Haller O, Staeheli P, Kochs G. 2007. Interferon-induced Mx proteins in antiviral host defense. Biochimie 89:812–818.

He B. 2006. Viruses, endoplasmic reticulum stress, and interferon responses. Cell Death Differ 13:393–403.

Hogue BG, Nayak DP. 1992. Synthesis and processing of the influenza virus neuraminidase, a type II transmembrane glycoprotein. Virology 188:510–517.

Hurtley SM, Bole DG, Hoover-Litty H, Helenius A, Copeland CS. 1989. Interactions of misfolded influenza virus hemagglutinin with binding protein (BiP). J Cell Biol 108:2117–2126.

Isler J, Skalet A, Alwine J. 2005. Human cytomegalovirus infection activates and regulates the unfolded protein response. J Virol 79:6890–6899.

Jordan R, Wang L, Graczyk T, Block T, Romano P. 2002. Replication of a cytopathic strain of bovine viral diarrhea virus activates PERK and induces endoplasmic reticulum stress-mediated apoptosis of MDBK cells. J Virol 76:9588–9599.

Kochs G, Janzen C, Hohenberg H, Haller O. 2002. Antivirally active MxA protein sequesters La Crosse virus nucleocapsid protein into perinuclear complexes. Proc Natl Acad Sci U S A 99:3153–3158.

Landis H, Simon-Jödicke A, Klöti A, Di Paolo C, Schnorr J, Schneider-Schaulies S, Hefti H, Pavlovic J. 1998. Human MxA protein confers resistance to Semliki Forest virus and inhibits the amplification of a Semliki Forest virus-based replicon in the absence of viral structural proteins. J Virol 72:1516–1522.

Limjindaporn T, Wongwiwat W, Noisakran S, Srisawat C, Netsawang J, Puttikhunt C, Kasinrerk W, Avirutnan P, Thiemmeca S, Sriburi R, Sittisombut N, Malasit P, Yenchitsomanus P. 2009. Interaction of dengue virus envelope protein with endoplasmic reticulum-resident chaperones facilitates dengue virus production. Biochem Biophys Res Commun 379:196–200.

Ludwig S, Pleschka S, Planz O, Wolff T. 2006. Ringing the alarm bells: signalling and apoptosis in influenza virus infected cells. Cell Microbiol 8:375–386.

Maruoka S, Hashimoto S, Gon Y, Nishitoh H, Takeshita I, Asai Y, Mizumura K, Shimizu K, Ichijo H, Horie T. 2003. ASK1 regulates influenza virus infection-induced apoptotic cell death. Biochem Biophys Res Commun 307:870–876.

Medigeshi G, Lancaster A, Hirsch A, Briese T, Lipkin W, Defilippis V, Früh K, Mason P, Nikolich-Zugich J, Nelson J. 2007. West Nile virus infection activates the unfolded protein response, leading to CHOP induction and apoptosis. J Virol 81:10849–10860.

Mibayashi M, Nakad K, Nagata K. 2002. Promoted cell death of cells expressing human MxA by influenza virus infection. Microbiol Immunol 46:29–36.

Morishima N, Nakanishi K, Takenouchi H, Shibata T, Yasuhiko Y. 2002. An endoplasmic reticulum stress-specific caspase cascade in apoptosis. Cytochrome c-independent activation of caspase-9 by caspase-12. J Biol Chem 277:34287–34294.

Morris SJ, Price GE, Barnett JM, Hiscox SA, Smith H, Sweet C. 1999. Role of neuraminidase in influenza virus-induced apoptosis. J Gen Virol 80 (Pt 1):137–146.

Morris SJ, Smith H, Sweet C. 2002. Exploitation of the Herpes simplex virus translocating protein VP22 to carry influenza virus proteins into cells for studies of apoptosis: direct confirmation that neuraminidase induces apoptosis and indications that other proteins may have a role. Arch Virol 147:961–979.

Naito T, Momose F, Kawaguchi A, Nagata K. 2007. Involvement of Hsp90 in assembly and nuclear import of influenza virus RNA polymerase subunits. J Virol 81:1339–1349.

Nakagawa T, Zhu H, Morishima N, Li E, Xu J, Yankner B, Yuan J. 2000. Caspase-12 mediates endoplasmic-reticulum-specific apoptosis and cytotoxicity by amyloid-beta. Nature 403:98–103.

Numajiri A, Mibayashi M, Nagata K. 2006. Stimulus-dependent and domain-dependent cell death acceleration by an IFN-inducible protein, human MxA. J Interferon Cytokine Res 26: 214–219.

Okuwaki M, Kato K, Nagata K. 2010. Functional characterization of human nucleosome assembly protein 1-like proteins as histone chaperones. Genes Cells 15:13–27.

Pavlovic J, Haller O, Staeheli P. 1992. Human and mouse Mx proteins inhibit different steps of the influenza virus multiplication cycle. J Virol 66:2564–2569.

Postigo A, Ferrer P. 2009. Viral inhibitors reveal overlapping themes in regulation of cell death and innate immunity. Microbes Infect 11:1071–1078.

Queitsch C, Sangster TA, Lindquist S. 2002. Hsp90 as a capacitor of phenotypic variation. Nature 417:618–624.

Rao R, Castro-Obregon S, Frankowski H, Schuler M, Stoka V, del Rio G, Bredesen D, Ellerby H. 2002a. Coupling endoplasmic reticulum stress to the cell death program. An Apaf-1-independent intrinsic pathway. J Biol Chem 277:21836–21842.

Rao R, Peel A, Logvinova A, del Rio G, Hermel E, Yokota T, Goldsmith P, Ellerby L, Ellerby H, Bredesen D. 2002b. Coupling endoplasmic reticulum stress to the cell death program: role of the ER chaperone GRP78. FEBS Lett 514:122–128.

Sadler A, Williams B. 2008. Interferon-inducible antiviral effectors. Nat Rev Immunol 8:559–568.

Sanders CJ, Doherty PC, Thomas PG. 2011. Respiratory epithelial cells in innate immunity to influenza virus infection. Cell Tissue Res 343:13–21.

Schneider-Schaulies S, Schneider-Schaulies J, Schuster A, Bayer M, Pavlovic J, ter Meulen V. 1994. Cell type-specific MxA-mediated inhibition of measles virus transcription in human brain cells. J Virol 68:6910–6917.

Schnorr J, Schneider-Schaulies S, Simon-Jödicke A, Pavlovic J, Horisberger M, ter Meulen V. 1993. MxA-dependent inhibition of measles virus glycoprotein synthesis in a stably transfected human monocytic cell line. J Virol 67:4760–4768.

Schultz-Cherry S, Hinshaw VS. 1996. Influenza virus neuraminidase activates latent transforming growth factor beta. J Virol 70:8624–8629.

Staeheli P, Haller O, Boll W, Lindenmann J, Weissmann C. 1986. Mx protein: constitutive expression in 3T3 cells transformed with cloned Mx cDNA confers selective resistance to influenza virus. Cell 44:147–158.

Stertz S, Reichelt M, Krijnse-Locker J, Mackenzie J, Simpson J, Haller O, Kochs G. 2006. Interferon-induced, antiviral human MxA protein localizes to a distinct subcompartment of the smooth endoplasmic reticulum. J Interferon Cytokine Res 26:650–660.

Stray SJ, Air GM. 2001. Apoptosis by influenza viruses correlates with efficiency of viral mRNA synthesis. Virus Res 77:3–17.

Su H, Liao C, Lin Y. 2002. Japanese encephalitis virus infection initiates endoplasmic reticulum stress and an unfolded protein response. J Virol 76:4162–4171.

Tardif K, Mori K, Kaufman R, Siddiqui A. 2004. Hepatitis C virus suppresses the IRE1-XBP1 pathway of the unfolded protein response. J Biol Chem 279:17158–17164.

Tardif K, Mori K, Siddiqui A. 2002. Hepatitis C virus subgenomic replicons induce endoplasmic reticulum stress activating an intracellular signaling pathway. J Virol 76:7453–7459.

Timofeeva TA, Klenk ND, Zhirnov OP. 2001. [Identification of the protease-binding domain in the N-terminal region of the influenza A virus matrix protein M1]. Mol Biol (Mosk) 35:484–491.

Turan K, Mibayashi M, Sugiyama K, Saito S, Numajiri A, Nagata K. 2004. Nuclear MxA proteins form a complex with influenza virus NP and inhibit the transcription of the engineered influenza virus genome. Nucleic Acids Res 32:643–652.

Urano F, Wang X, Bertolotti A, Zhang Y, Chung P, Harding H, Ron D. 2000. Coupling of stress in the ER to activation of JNK protein kinases by transmembrane protein kinase IRE1. Science 287:664–666.

Wang Y, Shen J, Arenzana N, Tirasophon W, Kaufman R, Prywes R. 2000. Activation of ATF6 and an ATF6 DNA binding site by the endoplasmic reticulum stress response. J Biol Chem 275:27013–27020.

Yoshida H, Haze K, Yanagi H, Yura T, Mori K. 1998. Identification of the cis-acting endoplasmic reticulum stress response element responsible for transcriptional induction of mammalian glucose-regulated proteins. Involvement of basic leucine zipper transcription factors. J Biol Chem 273:33741–33749.

Zamarin D, García-Sastre A, Xiao X, Wang R, Palese P. 2005. Influenza virus PB1-F2 protein induces cell death through mitochondrial ANT3 and VDAC1. PLoS Pathog 1:e4.

Zhirnov OP, Konakova TE, Garten W, Klenk H. 1999. Caspase-dependent N-terminal cleavage of influenza virus nucleocapsid protein in infected cells. J Virol 73:10158–10163.

Zhu C, Johansen F, Prywes R. 1997. Interaction of ATF6 and serum response factor. Mol Cell Biol 17:4957–4966.

Address correspondence to:
*Prof. Kyosuke Nagata*
*Department of Infection Biology*
*Graduate School of Comprehensive Human Sciences*
*University of Tsukuba*
*1-1-1 Tennodai*
*Tsukuba 305-8575*
*Japan*

*E-mail:* knagata@md.tsukuba.ac.jp

Received 28 September 2010/Accepted 5 July 2011

# Tamiflu-Resistant but HA-Mediated Cell-to-Cell Transmission through Apical Membranes of Cell-Associated Influenza Viruses

**Kotaro Mori**[◔], **Takahiro Haruyama**[◔¤], **Kyosuke Nagata***

Department of Infection Biology, Faculty of Medicine and Graduate School of Comprehensive Human Sciences, University of Tsukuba, Tsukuba, Japan

## Abstract

The infection of viruses to a neighboring cell is considered to be beneficial in terms of evasion from host anti-virus defense systems. There are two pathways for viral infection to "*right next door*": one is the virus transmission through cell-cell fusion by forming syncytium without production of progeny virions, and the other is mediated by virions without virus diffusion, generally designated cell-to-cell transmission. Influenza viruses are believed to be transmitted as *cell-free* virus from infected cells to uninfected cells. Here, we demonstrated that influenza virus can utilize cell-to-cell transmission pathway through apical membranes, by handover of virions on the surface of an infected cell to adjacent host cells. Live cell imaging techniques showed that a recombinant influenza virus, in which the *neuraminidase* gene was replaced with the *green fluorescence protein* gene, spreads from an infected cell to adjacent cells forming infected cell clusters. This type of virus spreading requires HA activation by protease treatment. The cell-to-cell transmission was also blocked by amantadine, which inhibits the acidification of endosomes required for uncoating of influenza virus particles in endosomes, indicating that functional hemagglutinin and endosome acidification by M2 ion channel were essential for the cell-to-cell influenza virus transmission. Furthermore, in the cell-to-cell transmission of influenza virus, progeny virions could remain associated with the surface of infected cell even after budding, for the progeny virions to be passed on to adjacent uninfected cells. The evidence that cell-to-cell transmission occurs in influenza virus lead to the caution that local infection proceeds even when treated with neuraminidase inhibitors.

**Citation:** Mori K, Haruyama T, Nagata K (2011) Tamiflu-Resistant but HA-Mediated Cell-to-Cell Transmission through Apical Membranes of Cell-Associated Influenza Viruses. PLoS ONE 6(11): e28178. doi:10.1371/journal.pone.0028178

**Editor:** Ron A. M. Fouchier, Erasmus Medical Center, The Netherlands

**Received** July 8, 2011; **Accepted** November 2, 2011; **Published** November 30, 2011



**Funding:** This work was supported in part by a grant-in-aid from the Ministry of Education, Culture, Sports, Science, and Technology of Japan (to KN: #20249025). The funders had no role in study design, data collection and analysis, decision to publish, or preparation of the manuscript. The authors received no additional external funding for this study.

**Competing Interests:** The authors have declared that no competing interests exist.

* E-mail: knagata@md.tsukuba.ac.jp

◔ These authors contributed equally to this work.

¤ Current address: Central Research Center, AVSS Corporation, Nagasaki, Japan

## Introduction

It is generally accepted that viruses, released as *cell-free* virions from an infected cell, transmit to distant cells and tissues. This spreading pathway contributes to wide-ranged diffusion of *cell-free* viruses. However, in this spreading pathway, viruses are exposed to host anti-virus defense systems. In contrast, direct infection to a neighboring cell is considered to be beneficial for the virus in terms of evasion from the host anti-virus defense. There are two typical manners in infection to "*right next door*": one is the virus transmission through cell-cell fusion by forming syncytium without production of progeny virions, and the other is mediated by virions without virus diffusion, generally designated cell-to-cell transmission [1,2].

The cell-cell fusion infection pathway is characteristic for a variety of virus such as paramyxoviruses, herpesviruses, some retroviruses, and so on. For example in the case of measles virus belonging to *Paramyxoviridae*, infection is initiated by the interaction of the viral hemagglutinin glycoprotein with host cell surface receptors. The virus penetrates into the cell through membrane fusion mediated by the interaction of the fusion glycoprotein. In later stages of infection, newly synthesized glycoproteins accumulate at the cell membrane resulting in fusion of the infected cell with neighboring cells by producing syncytia. Thus, viruses can spread from cell to cell without producing *cell-free* virus particles.

The examples of the cell-to-cell transmission are diverse, and these mechanisms are dependent on pairs of viruses and host cells. Vaccinia virus particles bound on the filopodium of an infected cell are repelled toward neighboring uninfected cells by the formation of filopodia using actin filament [3]. The filopodia direct viruses to uninfected cells. Immunotropic viruses including retroviruses utilize an immunological synapse, designed as virological synapses for the cell-to-cell transmission [4–7]. Claudin-1 and occludin, components of tight junction, are involved in hepatitis C virus (HCV) entry through the cell-to-cell transmission [8,9]. The cell-to-cell transmission through tight junction is also observed in other viruses which infect epithelial layers [10,11]. These retroviruses and HCV remain on the surface of an infected cell even after budding. The uninfected cells adjacent to these infected cells can accept or take over viruses from